Numerical Study of a Separated Boundary Layer Transition over Two and Three Dimensional Geometrical Shapes

[1]HAYDER AZEEZ DIABIL , [1]XIN KAI LI , [2]IBRAHIM ELRAYAH ABDALLA
[1]Engineering Science and Advanced System Department
De Montfort University
Leicester, LE1 9BH
UK
[2]Jubail University College
Jubail Industrial City, 31961
K.S.A
P13003950@my365.dmu.ac.uk

Abstract: - The current study sheds a light on two fundamental aspects of a transitional separated-reattached flow induced over a two-dimensional blunt flat plate and three-dimensional square cylinder employing large eddy simulation conducted with Open FOAM CFD code. These aspects are different vortices shedding frequency modes and large scale structures and their development. The current paper is the first study to investigate a transitional separated-reattached flow in a three-dimensional square cylinder and compare between transition aspects of this case and that in a two-dimensional flat plate. It is not clear whether all transitional separated-reattached flows have low frequency shear layer flapping and selective high shedding frequency. This issue is addressed. The current LES results show that the characteristic shedding frequency value for the square cylinder is different from that in the flat plate. Coherent structures and their development are visualized at different stages of transition for both geometers. In the square cylinder, Kelvin-Helmholtz rolls are twisting around this geometry and evolve topologically to form hairpin structures. In the flat plate, Kelvin-Helmholtz rolls stay flat and hairpin structures formed by a braking down process.

Key-Words: - Separated-reattached flow, Transition, Shedding frequency modes, Coherent structures, Flow visualization, Large eddy simulation

1 Introduction

Well understanding of separated boundary layer is important due to its dramatic changes in drag force, lift force, and heat transfer rate in many practical engineering applications either the flow is internal such as diffusers, combustors and channels with sudden expansions or it is external such as flow around airfoils, projectiles, vehicles and buildings. Separated boundary layer which involves a transition from laminar to turbulence is more complicated than transition in attached flow where aspects of transition in the separated layer are not achieved yet and still a big challenge [1].

Separation of flow takes place either the flow encounters a strong adverse pressure gradient or there is an obstacle within the flow. In the first separation case, the momentum in the boundary layer is not high enough to overcome the pressure gradient and both separation and reattachment locations change as flow parameters vary [2]. In the other case, the separation location is fixed on surface of obstacle which may be a flat plate, hump, forward/ backward facing step.

If the separated boundary layer reattaches to a solid surface, a separated-reattached flow will be formed and a separation bubble will be constructed. Separation bubble is a parasitic in aerodynamic applications because it increases drag force which reduces efficiency and stability of these applications. Consequently, instability results had been experimentally observed to reduce aerodynamic performance as well as result in potentially dangerous dynamic structural loading in aerospace structures [3] and [4].

Three types of separated-reattached flows are laminar, turbulent, and transitional. In laminar separated-reattached flow, both separated and reattached flows are laminar while in turbulent separated-reattached flow, both separated and reattached flows are turbulent. In transitional separated-reattached flow, a laminar flow at relatively low Reynolds number separates forming a

laminar free shear layer. The separated laminar layer becomes unstable and has a tendency to undergo transition to turbulence flow that reattaches to the solid surface. In this type of separated-reattached flow, the separation bubble is susceptible to be unstable due to its sensitive to small fluctuations in upstream flow [4] and [5].

The current study sheds a light on two fundamental aspects of the transitional separated-reattached flow are different shedding frequency modes and large scale structures and their development.

Three frequency modes of separated-reattached flows which investegated in many previous studies: low frequency mode, characteristic (regular) frequency shedding mode, and selective high frequency mode. The low frequency mode is related to the dynamic of the separation bubble growth/decay that so called in literature as low frequency shear layer flapping [6], [7], and [8]. The characteristic frequency shedding mode is interpreted as characteristic shedding frequency of the large-scale structures from the free shear layer of the separation bubble. Selective high-frequency shedding from the separated shear layer is found to be connected to the low-frequency motion in the shear layer [8].

Power spectra for the velocity and surface pressure fluctuation of experimental study in Kiya and Sasaki [6] estimated that the low frequency shear layer flapping value to be of the order 0.12 U_0/x_R (where U_0 is the free stream velocity and x_R is the mean reattachment length) at a position close to the separation line. Separated-reattached flow in this work was turbulent and induced over a blunt flat plate. The authors suggested that flapping of the shear layer was a result of unsteadiness of the large structures that was related to the shrinkage and enlargement of the separation bubble. In this experiment, value of the characteristic shedding frequency of the large-scale structures from the free shear layer of the separation bubble was detected to be 0.6-0.8 U_0/x_R. For similar geometry and nature of separated flow, Hillier and Cherry [9] and Cherry et al. [7] showed that 0.12 U_0/x_R as a value of the low frequency shear layer flapping where they confirmed the value of this phenomenon that reported in [6]. Spectra of velocity and surface pressure fluctuation in Cherry et al. [7] presented that the dominant characteristic shedding frequency was 0.7 U_0/x_R. They concluded that the low frequency shear layer flapping was an integral feature of a fully turbulent separated flow.

This conclusion was supported in Abdalla and Yang [10] study for similar geometry. They emphasised that there was no low frequency shear layer flapping in their study which investigated transitional separated-reattached flow. They attributed that the absence of this phenomenon was due to the action of the laminar part of separation bubble which acted as a filter to absorb and damp this low frequency. Another support of Cherry et al. [7] conclusion reported in many studies that investigated a turbulent separated-reattached flow on different geometries. Lee and Sung [11] revealed the low frequency shear layer flapping close to the separation line in addition to the characteristic shedding frequency mode in a backward facing step flow. This phenomenon was detected in separated flow on a flat plate with a long central splitter plate [12] and [13]. However, for similar flow configuration, no dominant modes of frequencies were observed by the power spectra in [14].

On the other hand, studies of Yang and Voke [15] and Ducoine et al. [16] that carried out numerically may disprove the conclusion of Cherry et al. [7] who emphasised that a fully turbulent separation was a condition of the low frequency shear layer flapping. Yang and Voke [15] revealed the low frequency shear layer flapping with a value of 0.104 U_0/x_R took place close to the separation line of a transitional separated-reattached flow generated on a flat plate with a semicircular leading edge where the separated flow was a laminar in nature. The authors suggested that the presence of this phenomenon was due to a big vortex shedding which occurred at a lower frequency. It was reported in this study that the regular shedding frequency varied in the range of 0.35 U_0/x_R to 1.14 U_0/x_R. The averaged frequency was estimated at about 0.77 U_0/x_R.

Ducoine et al. [16] investigated the transition to turbulence over a wing section. The spectrum showed that Setrouhal number value of 0.08 was estimated to be the magnitude of the shear layer flapping in the laminar separation part. In this study, it was documented that there were two characteristic shedding frequencies of the large-scale structures from the separation bubble associated with 0.12 and 0.248 values of Setrouhal number.

Tafti and Vanka [8] identified 0.15 U_0/x_R as a value of the low frequency shear layer flapping of a turbulent separated shear layer on a blunt flat plate. They suggested that this phenomenon was due to the periodic enlargement and shrinkage of the separation bubble. They observed a selective high-frequency mode that was found to occur with a period equal to that of the low frequency unsteadiness. The selective high-frequency mode was reported for the first time in Tafti and Vanka [8]

and its value was 4.2 U_0/x_R which was exactly seven times the characteristic frequency shedding mode which found as 0.6 U_0/x_R. Tafti and Vanka [8] documented that the selective high frequency mode is more notable with low Reynolds numbers. Such selective high-frequency mode was observed by spectra for the velocity components in [10] for a transitional separated-reattached flow on a blunt flat plate. The magnitude of this selective high frequency was reported as 5-6.5 U_0/x_R which was approximately seven times higher than the regular shedding frequency that was equivalent to 0.7-0.875 U_0/x_R.

In many if not all turbulent and transitional flows, presence of large scale structures (coherent structures) is common. Coherent structures are defined as spatially coherent and temporally evolving vortical structures [17]. Another definition of coherent structure reported in Hussain [18] as a connected large-scale turbulent fluid mass with a phase-correlated vorticity over its spatial extent. Robinson [19] defined coherent structure as a three-dimensional region of the flow over which at least one fundamental flow variable (velocity component, density, etc) exhibited significant correlation with itself or with another variable over a range of space and/or time that was significantly larger than the smallest local scales of the flow. Many types of coherent structures are presented in literature such as Kelvin-Helmholtz rolls, streaks, lambda-shaped, hairpin, horseshoe, counter-rotating, and ribs.

Understanding of coherent structures construction and their evolution may improve our knowledge of the transition mechanisms as well as turbulence development after the transition. Well knowledge of the dynamics of the structures of the turbulence may enhance many features of this flow such as mixing, heat and mass transfer, chemical reaction, and combustion in addition to development of an applicable modelling of turbulence [20]. So, paying more attention to study the coherent structures is needed.

Scales and shapes of coherent structures are different from flow to flow depending on flow geometry, flow condition and location with respect to solid surface [21]. Large-scale spanwise vortices were found to be regular coherent structures in plane mixing layer flows [22]-[25]. Robinson [19] and Perry and Chong [26] reported that hairpin or horseshow vortices were dominant large-scale motions in turbulent boundary layer while for same flow, streaky structures appeared to be the coherent structures in [27]-[30]. On the other hand, dominant structures of flow dynamics in wakes were counter-rotating vortices [31]-[33].

Many techniques have been developed to extract the coherent structures from turbulent and transitional flows: conditional, non-conditional, pattern recognition, and flow visualisation. Due to using flow visualisation technique in the current study, many of studies that employed this technique will be presented here. For other techniques, the reader should refer to [34] and [35] for conditional methods, [36] and [37] for non-conditional methods, and [31] and [32] for pattern recognition technique.

Basically, there are three flow visualization techniques: low-pressure isosurface, vorticity field isosurface, and Q-criterion isosurface. Robinson [19] employed low-pressure isosurface to investigate development of coherent structures in a turbulent boundary layer. Streamwise vorticity isosurface was used by Comte et al. [23] to reveal coherent structures in a turbulent mixing layer flow. Comparison between these schemes shows that the low-pressure isosurface was more active than the vorticity field isosurface to illustrate coherent structures of flow with presence of a solid surface due to a high shear compared to vortical intensity of vortices that located close to the solid surface.

Q-criterion scheme, that shares some properties from the vorticity and pressure criterion, was used by Karaca and Gungor [38] and Gungor and Simens [39] to reveal evolution and breaking down of the coherent structures of the transitional-separated reattached flow on an airfoil under effect of adverse pressure gradient. The aim of these studies was focus on the effect of surface roughness on location of breaking down of large structures within the separation bubble. However, description of the coherent structures and their spatial and temporal evolution were not presented in their studies. Ducoin et al. [16] studied instability mechanisms of transition to turbulence of a separated boundary-layer flow over an airfoil at low angle of attack using SD7003 wing section under effect of adverse pressure gradient. They showed that in unstable region of separation bubble, two-dimensional Kelvin–Helmholtz rolls constructed and deformed to C-shape structures. Further downstream, these structures shed from the separation bubble when vortex filaments in the braid breaking region.

For separated-reattached flow over obstacles mounted in an oncoming stream, Yang and Voke [15] observed forming hairpin structures in the transitional separated-reattached flow induced on a flat plate with a semi-circular leading edge. It was reported in this study that the large motions started as two-dimensional Kelvin-Helmholtz rolls separated from the unsteady free shear layer. The rolls grew downstream and distorted to form

spanwise peak-valley structures. Rolling up of the peak-valley structures formed three-dimensional streamwise hairpin structures around the reattachment zone. The method of flow visualization that used in this study was low pressure isosurface. Similar technique was used in Abdalla and Yang [40] to reveal coherent structures of a transitional separated-reattached flow over a flat plate with a rectangular leading edge. The authors postulated that the spatial and temporal evolution of those rolls were their pairing with each other and stretching in the streamwise direction forming three-dimensional hairpin and ribs structures. Around the reattachment zone, the new three-dimensional structures shed to the turbulent attached flow and broke down into smaller structures further downstream.

Abdalla et al. [41] presented a study to show shapes of structures of transitional separated-reattached flow on a two-dimensional surface mounted obstacle and forward-facing step using low pressure isosurface method. For both geometries, there was a forming of a large size roll by merging of two Kelvin–Helmholtz rolls. Direct braking down of the large rolls was detected to form horseshoe vortices where there was no existence of hairpin structures that dominated as coherent structures of separated-reattached flows on flat plates. The authors documented that the instability mechanism that led to form three-dimensional structures was different from that in the flat plate case and more research is needed to reveal this instability mechanism.

It seems that in the literature, identification of shedding frequencies modes, coherent structures, and their development of a transitional separated-reattached flow are not well established yet and more efforts are needed to cover these issues. In addition, a two-dimensional geometrical shape was selected to be a test case in all studies which investigated this flow.

The question that arise is; if the transitional separated-reattached flow is induced around a three-dimensional square cylinder, is there any similarity between its transition fundamental features and those which investigated in the previous studies? Current study may be the first work that may answer this question. In addition, it presents a comparison between transition aspects of a transitional separated-reattached flow that is generated on a two-dimensional blunt flat plate and three-dimensional square cylinder by a numerical simulation is implemented in the Open FOAM (open source CFD toolbox and hereinafter OF) employing large eddy simulation (hereafter LES) with dynamic subgrid-scale model.

The outline of this paper is definition of governing equations in section 2, description of numerical computations in section 3, validation of the current Open FOAM code in section 4, illustration of transition process in section 5, analysing the velocity components and pressure spectra in section 6, and shedding a light on coherent structures and their development in section 7.

2 Governing equations

Navier-Stokes equations govern motions of all Newtonian fluids. To solve these equations by using direct numerical simulation method, a very high resolution of numerical grid is required to capture all length scales; and a very small time step is employed to capture all time scales of the flow. For relatively high Reynolds number and/or complex geometries, this method is expensive and sometimes impossible due to a broad range of length and time scales included in some problems. To reduce the computational cost, large eddy simulation (LES) method is employed. In this approach, large eddies or large scale motions (grid-scale) are computed directly and small eddies (subgrid-scale) are modelled. A spatial filter is used to separate the flow to resolved (grid-scale) part and unresolved (subgrid-scale) part. So, any instantaneous variable (g) can be expressed as

$$g_i = \bar{g}_i + g_i' \tag{1}$$

where $\bar{g}_i$ is the grid-scale and g_i' is the subgrid-scale.

If the finite volume method is used to solve the LES equations, these equations are integrated over control volumes and the governing equations can be regarded as implicitly filtered that are equivalent to imposing a top-hat filter. In this case, the local grid spacing is considered as a local filter width [21]. The filtered continuity and Navier-Stokes equations for incompressible Newtonian flow of LES are

$$\frac{\partial \overline{u}_j}{\partial x_j} = 0 \tag{2}$$

$$\frac{\partial \overline{u}_i}{\partial t} + \frac{\partial \overline{u}_i \overline{u}_j}{\partial x_j} = -\frac{1}{\rho}\frac{\partial \overline{p}}{\partial x_i} + \upsilon \frac{\partial^2 \overline{u}_i}{\partial x_j \partial x_j} - \frac{\partial \tau_{ij}}{\partial x_j} \tag{3}$$

where u_i, u_j $(i, j = 1, 2, 3)$ are the three velocity components in Cartesian form, p denotes pressure, ρ denotes density, and υ denotes kinematic viscosity.

Overbar notation denotes application of the spatial filtering which is called grid-scale filter. The unresolved subgride-scale stress $\tau_{ij} = \overline{u_i u_j} - \overline{u}_i \overline{u}_j$ is modeled by an eddy viscosity model. According

to Boussinesq approximation, there is a relationship between the grid-scale strain rate tensor and the residual stress tensor (τ_{ij}) that refers to the effect of subgrid-scale motions on the resolved fields which can be expressed as

$$\tau_{ij} = -2\,\upsilon_t\,\overline{S}_{ij} + \frac{1}{3}\,\delta_{ij}\,\tau_{kk} \quad (4)$$

where

$$\overline{S}_{ij} = \frac{1}{2}\left(\frac{\partial \overline{u}_i}{\partial x_j} + \frac{\partial \overline{u}_j}{\partial x_i}\right) \quad (5)$$

δ_{ij} is the Kronecker delta which is 1 if $i = j$ and zero if $i \neq j$, υ_t is the subgrid-scale eddy viscosity, $\overline{S}_{ij}$ is the grid-scale strain rate tensor, and τ_{kk} is the isotropic part of the stress tensor that not modeled and added to the pressure term. Equation (3) can be re-written as

$$\frac{\partial \overline{u}_i}{\partial t} + \frac{\partial \overline{u}_i \overline{u}_j}{\partial x_j} = -\frac{1}{\rho}\frac{\partial p^*}{\partial x_i} + \upsilon\frac{\partial^2 \overline{u}_i}{\partial x_j \partial x_j} + 2\frac{\partial \upsilon_t \overline{S}_{ij}}{\partial x_j} \quad (6)$$

where

$$p^* = \overline{p} - \frac{1}{3}\rho\,\delta_{ij}\,\tau_{kk} \quad (7)$$

The remaining problem in equation (6) is to solve the subgrid-scale eddy viscosity υ_t. The oldest and simplest model to solve the subgrid-scale eddy viscosity was proposed by Smagorinsky

$$\upsilon_t = C\,\Delta^2\,|\overline{S}|, \quad |\overline{S}| = \sqrt{2\,\overline{S}_{ij}\,\overline{S}_{ij}} \quad (8)$$

where C is a parameter in the model and Δ is the grid filter scale (filter width) that equals to the cubic root of the cell volume $(\Delta x \Delta y \Delta z)^{\frac{1}{3}}$. From equations (4) and (8), the subgrid-scale stress (τ_{ij}) can be written now as

$$\tau_{ij} = -2\,C\,\Delta^2\,|\overline{S}|\,\overline{S}_{ij} + \frac{1}{3}\,\delta_{ij}\,\tau_{kk} \quad (9)$$

In the Smagorinsky model, $C = C_s^2$, where C_s is the Smagorinsky constant. The specification of proper value for the Smagorinsky constant is actually a controversial topic, none of the alternative values are entirely satisfactory. Despite this, the majority of works in the literature are assume that the Smagorinsky constant is taken as 0.18 for isotropic turbulent flow and is reduced to 0.1 for flow near the solid wall [42].

There are many shortcomings of the Smagorinsky model, for example, it is too dissipative (so it is not suitable to simulate the transitional flows) and the Smagorinsky constant needs to be adjusted for different flows [42] and [43]. To overcome these, a dynamic subgrid-scale model was developed by Germano et al. [44]. In this model, the constant C determined locally in space and in time during the calculation progress and hence, adjusting the model coefficient artificially is avoided. The procedure of calculation of dynamic subgrid-scale coefficient is described in [44] and [45].

3 Numerical computations

The computational mesh and conceptual representation of the computational domain for the two-dimensional flat plate and three-dimensional square cylinder are shown in Figs. 1 and 2 respectively. Details of the computational domain for both geometrical shapes are shown in Tables 1 and 2. The inflow boundary and outflow boundary are at (x/D=4.5) and (x/D=20.5) respectively distance from the leading edge of both geometries. The lateral boundaries are at 8D distance from the centerline (y = 0), corresponding to a blockage ratio of 16. The domain spanwise dimension is 4D.

The numerical simulation is performed using a structured mesh with 198×220×84 cells distributed along the streamwise, wall-normal, and spanwise directions. Frictional velocity in place that is close to the outlet boundary is similar approximately for both geometries. So, mesh cells sizes in terms of wall unites based on the frictional velocity downstream of the reattachment at x/D = 18 is similar for both geometries. In streamwise direction, the cell size varies from $\Delta x^+ = 4.86$ to $\Delta x^+ = 26.417$, and in wall normal direction, it varies from $\Delta y^+ = 0.739$ to $\Delta y^+ = 30.49$. A uniform grid size is used in the spanwise direction $\Delta z^+ = 4.88$. The time step $\Delta t = 2\times10^{-6}$ sec is used in the time iterations, which equivalents 0.001885 D/U_0 where U_0 is the inflow velocity for both geometries corresponding to a CLF_{max} number of 0.31 for the flat plate and 0.26 for the square cylinder, where CFL (Courant-Friedrich-Lewy) number is defined as

$$CFL = \Delta t\left(\frac{|u|}{\Delta x} + \frac{|v|}{\Delta y} + \frac{|w|}{\Delta z}\right) \quad (10)$$

For both geometries, the simulation ran for about 8 flows passes through the domain (100,000 time steps) to allow the transition and turbulent boundary layer to be well-established, i.e. the flow to have reached a statistically stationary state. The averaged results were gathered over a further about 30 flows passes through the domain (400,000 time steps). Total time of the simulation is 1 sec (942.5 D/U_0) corresponding to about 38 flows passes or residence times.

Reynolds number of the current study is 6.5×10^3 based on the thickness of the plate and the inflow velocity that is uniform, aligned with the plate, and equals 9.425m/sec. Zero velocity gradient is used at the outflow boundary. No-slip boundary conditions are applied at all walls. In the lateral boundaries, free-slip boundary conditions are used. For the flat

plate, periodic boundary conditions are applied at the spanwise direction where the flow is assumed to be statistically homogenous. This boundary condition is changed to free-slip for the square cylinder.

In the current study, large eddy simulation conducted with OF 2.4.0 (open source CFD toolbox) is employed with using of dynamic sub-grid scale model. In OF, the governing equations of large eddy simulation discretized using the finite volume method. In the current study, the second order implicit backward temporal scheme is used for the time advancement. The Second order central differencing scheme is used for spatial discretisation. Mass conservation is imposed through the pressure-velocity by coupling method which is calculated by pressure implicit with splitting of operators (PISO) algorithm [46].

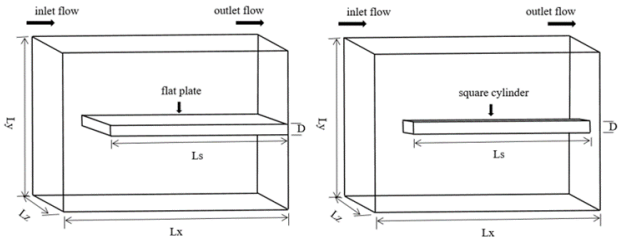

Fig.1 Conceptual representation of the domain for the two-dimensional flat plate and three-dimensional square cylinder

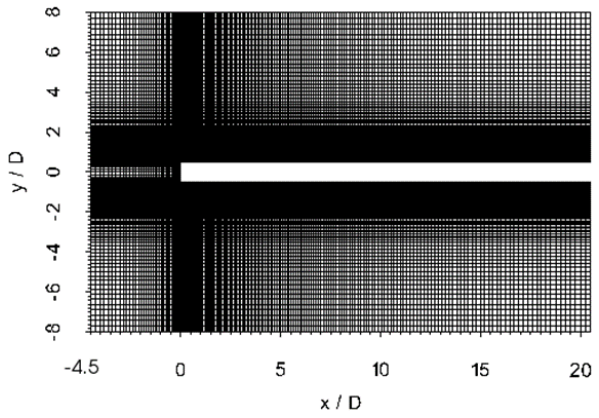

Fig.2 Computational mesh at the mid-distance of the spanwise direction for both geometrical shapes

Table 1 Domain size for both geometrical shapes

Lx	25 cm
Ly	16 cm
Lz	4 cm
blockage ratio	16

Table 2 Dimensions of both geometrical shapes

	flat plate	square cylinder
Thickness (D)	1 cm	1 cm
Length (Ls)	20.5 cm	20.5 cm
width	4 cm	1 cm

4 Results and discussion

The geometry and Reynolds number of the flat plate in the current study are similar to that used in the experimental study of Castro and Epik [47] and the numerical study of Yang and Abdalla [48]. In [47], the blockage ratio was higher than the present blockage ratio and a flap was used to control the reattachment length. The main purpose of the experimental work of Castro and Epik [47] was study the turbulent boundary layer after the reattachment. Due to results of the separation bubble in this experimental work were limited, results of another experimental work in [6] chosen here. Kiya and Sasaki [6] investigated turbulent separated-reattached flow on a flat plate with blunt leading edge with Reynolds number (26×10^3) was higher than the current Reynolds number. There was no transition within this experimental work and the blockage ratio was higher than the current blockage ratio.

An important parameter in the separated-reattached flow is the mean reattachment length (x_R). According to the definition of Le et al. [49], the mean reattachment point is the streamwise location of the first grid point from the wall where the value of the mean streamwise velocity equals zero (U_m=0). Profile of streamwise mean velocity at the first cell from the wall along the streamwise direction for both geometries are shown in Fig. 3. It is clearly shown that the mean reattachment length is x_R= 6D for the flat plate and x_R= 3.4D for the square cylinder.

The time averaged velocity vectors for both shapes at the mid-distance of the spanwise direction z/D=2 are shown in Fig. 4. It is clearly found that there is a one separation bubble starts from the leading edge at x/D=0 and ends downstream at about x/D=6 for the flat plate and x/D=3.4 for the square cylinder. In General, the size of the separation bubble, in terms of height and length, for the flat plate is much larger than one in the square cylinder, which is clearly shown in Fig. 4.

For the flat plate case, the current mean reattachment length 6D is lower than 7.7D as a measured mean reattachment length in [47]. This is a good agreement can be taken with consideration of effects of the flap and higher blockage ratio of

Castro and Epik [47]. Despite the mean reattachment length of the current flat plate case is lower than 6.5D as a predicted length of a separation bubble in [48], this is a good agreement if different characteristics of the current OF commercial code and the FORTRAN code that used in Yang and Abdalla [48] have been concerned. Simulated results of Yang and Abdalla [48] presented by employing a staggered numerical mesh while a co-located numerical mesh is used in the current simulation. In addition to the difference between the numerical scheme that used in [48] and PISO algorithm in the current study, may be a cause of the difference on the mean reattachment lengths.

The mean reattachment length of the experimental work of Kiya and Sasaki [6] is 5.05D, which is lower than the current mean reattachment length of the flat plate. However, this experimental work was investigated based on separated flow which was fully turbulent in nature with a higher Reynolds number (26×103) compared with the current Reynolds number. It is interesting to note that with decreasing of the Reynolds number below (30×103), the separation bubble length is increased [7]. Therefore, the current mean reattachment length is consistent with experimental observations in [6]. However, the good agreement between the current results and other results confirms the ability of the OF to simulate the transitional separated-reattached flow.

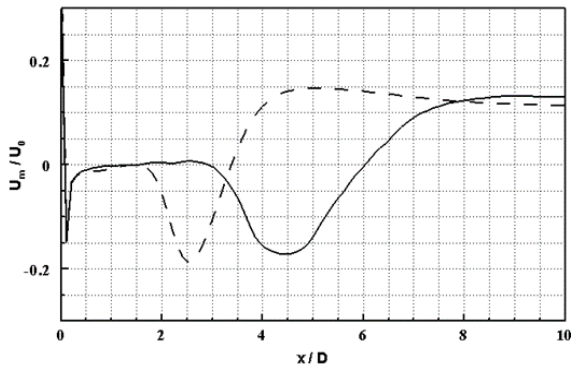

Fig.3 Profile of streamwise mean velocity normalized by inflow velocity at the first cell from the wall along the streamwise direction: solid line for the flat plate and dashed line for the square cylinder

Comparisons among the mean values of the flow for the flat plate case of the current study and results of the experimental work in [6] and numerical simulation in [48] are presented in Figs. 5-7. In these figures, profiles of the mean values of the flow are plotted at five positions of streamwise direction distributed at: x/xR=0.2, 0.4, 0.6, 0.8, and 1. The vertical axis of these figures is the wall normal direction normalized by the reattachment length (y/xR) starts from the surface of the plate. As shown in Fig. 2, the center of the plate is the original point of the lateral direction. This location is shifted to the surface of the plate for all profiles of the flow mean values that shown in Figs. 5-7.

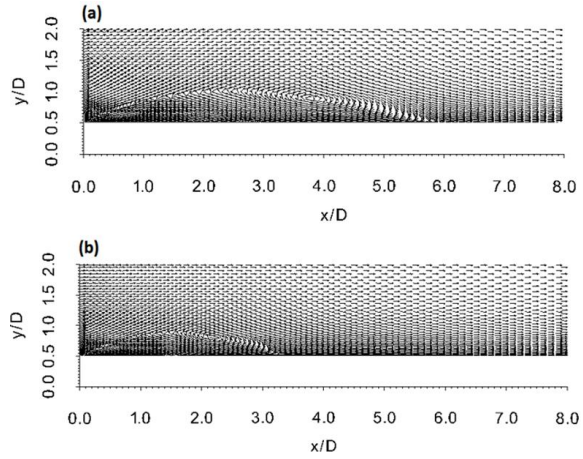

Fig.4 Time averaged velocity vectors: (a) the flat plate, (b) the square cylinder

Profiles of the mean streamwise velocity normalized by the free stream velocity (Um/U0) are shown in Fig. 5. Despite the current peak at the first position is slightly lower than the peak in Yang and Abdalla [48], an excellent agreement between both studies results can be observed in Fig. 5. In addition, in this figure, a good agreement with results of the experimental work in [6] can be seen. However, the difference is coming from three main reasons. The first reason is difference in the separated flow nature, where in the current study it is laminar while in the experimental work it was turbulent. Difference in the blockage ratio can be considered as the second reason, where the current blockage ratio is 16 and it was 20 in [6]. The third reason is the low current Reynolds number compared to the Reynolds number in the experimental work in [6].

Figure 6 shows profiles of root mean square fluctuating streamwise velocity normalized by the free stream velocity (u'rms/U0). Generally, it can be observed a very good agreement between the current results and data of Yang and Abdalla [48]. However, the peak in [48] at the fourth and fifth positions is slightly lower than peak of the current results. Due to turbulent separated flow in [6], peaks of root mean square fluctuating streamwise velocity are higher than current peaks at the first and second locations.

Current Reynolds shear and normal stresses normalized by the free stream velocity at the reattachment point are shown in Fig. 7. Results of experimental work in [47] at Reynolds number which equals to the current Reynolds number is presented in this figure. Good agreement between the current results and results of Yang and Abdalla [48] can be seen in this figure. Reynolds shear stress in [6] is higher than the current Reynolds shear stress as shown in Fig. 7. The three causes that described in Fig. 5 can be considered here for this difference.

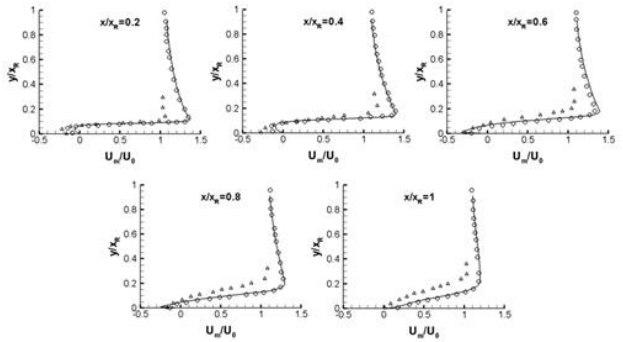

Fig.5 Profiles of mean streamwise velocity, solid line: current results, circles: Yang and Abdalla (2009), triangles: Kiya and Sasaki (1983)

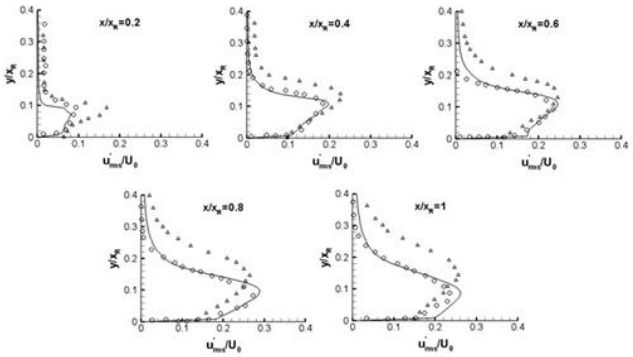

Fig.6 Profiles of root mean square fluctuating streamwise velocity, solid line: current results, circles: Yang and Abdalla (2009), triangles: Kiya and Sasaki (1983)

In Fig. 7, peaks of all Reynolds stress profiles in [47] are lower than current peaks of these profiles. These Differences are coming from three reasons. The first reason is difference in the blockage ratio, where in Castro and Epik [47], it was larger than the current blockage ratio by about four times. Using a flap to control the reattachment length in [47] can be considered as the second reason. The third reason is the results that measured at the reattachment point in [47] were at Reynolds number value of 3.68×103 because of the upper velocity limit (6m/sec) on the miniature pulsed-wire probe. Castro and Epik [47] documented that the value of the Reynolds stresses at Reynolds number of 6.5×103 were higher than that presented in Fig. 7 by 12%. So, a good agreement can be considered between the current data and results of the experimental work in [47].

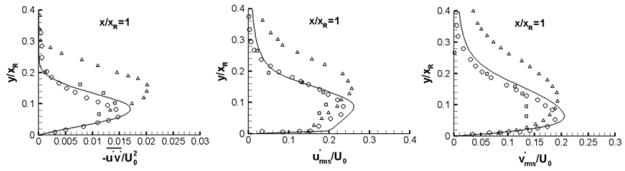

Fig.7 Profiles of Reynolds shear and normal stresses at the reattachment point, solid line: current results, circles: Yang and Abdalla (2009), triangles: Kiya and Sasaki (1983), squares: Castro and Epik (1998)

It should be noted that, to the best knowledge of the authors, the current study is the first paper to present results of the transitional separated-reattached flow over the three-dimensional square cylinder. There are no results of this geometry presented in the literature. Therefore, the mean values of the flow of this three-dimensional shape are presented here without a comparison with another published work.

From Figs. 5-7, it is found that the current OF code presents reasonably accurate results and it can be used to simulate the transitional separated-reattached flow over the three-dimensional square cylinder.

For the current flat plate and square cylinder, the mean value profiles of the flow normalized by the inlet velocity are shown in Figs. 8 and 9. The mean values of the flow are plotted at similar values of (x/x_R) that chosen in Figs. 5 and 6 and the wall normal axis is normalized by the reattachment length too. The origin point is shifted to the top surface of the square cylinder.

There is a similar behavior of the mean streamwise velocity profile for both geometrical shapes as shown in Fig. 8. For all streamwise locations, the maximum value of the mean streamwise velocity of the two-dimensional flat plate is higher than its value of the three-dimensional square cylinder by about 18%. Root mean square fluctuating streamwise velocity profiles for both geometrical shapes are shown in Fig. 9. It can be seen there is a similar behavior of these velocities profiles for both geometrical shapes with just difference in the peak values. Generally, the peak value of this variable for the flat plate is higher than its value for the square cylinder by about (20%-25%).

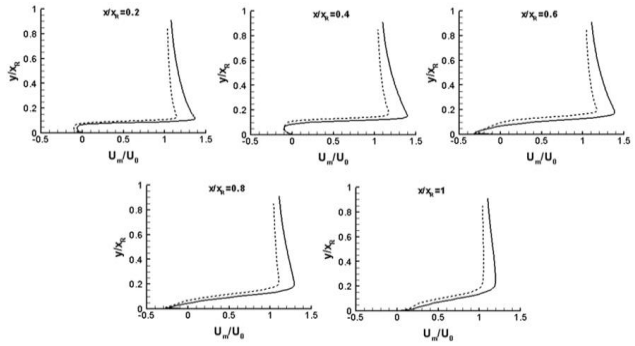

Fig.8 Mean streamwise velocity profiles of the flow: solid line for the flat plate and dashed line for the square cylinder

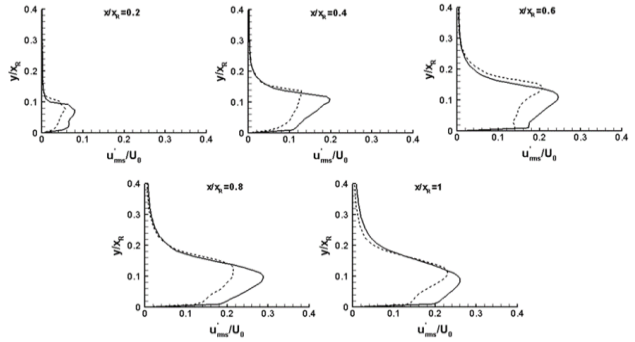

Fig.9 Root mean square fluctuating streamwise velocity profiles of the flow: solid line for the flat plate and dashed line for the square cylinder

5 Transition process

The transition processes for the two geometries are illustrated in Fig. 10 for the flat plate and Fig. 11 for the square cylinder by using x-y plane of instantaneous spanwise vorticity at the mid spanwise direction taken at three different times. It can be seen that a separated two-dimensional laminar layer is formed at the leading edge for both geometries. Two-dimensional spanwise vortices, named Kelvin-Helmholtz rolls are formed in the free shear layer that becomes inviscidly unstable. Because of presenting and growing any small disturbance downstream, the two-dimensional spanwise vortices are distorted and changed to be the three-dimensional streamwise vortices which are associated with a three-dimensional motion. Furthermore, close to the reattachment location, the three-dimensional structures are shed to the turbulent boundary layer that develops rapidly before reaching to the outflow boundary. This phenomenon can be clearly seen in Figs. 32 and 33.

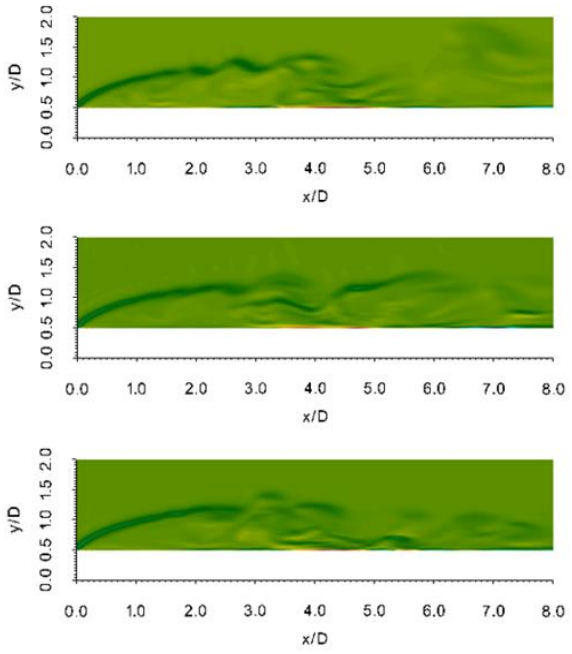

Fig.10 x-y plane of instantaneous spanwise vorticity development for the flat plate

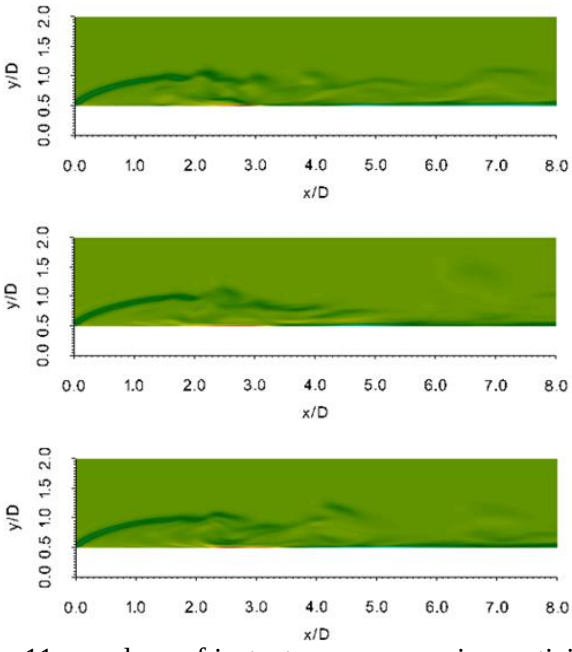

Fig.11 x-y plane of instantaneous spanwise vorticity development for the square cylinder

In the case of the square cylinder, four separation bubbles are constructed on the top, down, and sides surfaces in the square cylinder. The instantaneous spanwise vorticity isosurface on the top and side surfaces of the square cylinder are plotted with sequential times in Fig. 12. It is clearly seen that there is a laminar separated layer starting from the leading edge of each surface for a two-dimensional laminar flow. At a specific location, this layer becomes more turbulent and evolves to three

dimensionality state as an indication to the flow at the transition stage. Further downstream, the reattachment of the flow takes place and develops to be a turbulent attached flow. Clearly, there is no considerable difference of the flow development on each surface for the square cylinder as shown in Fig. 12.

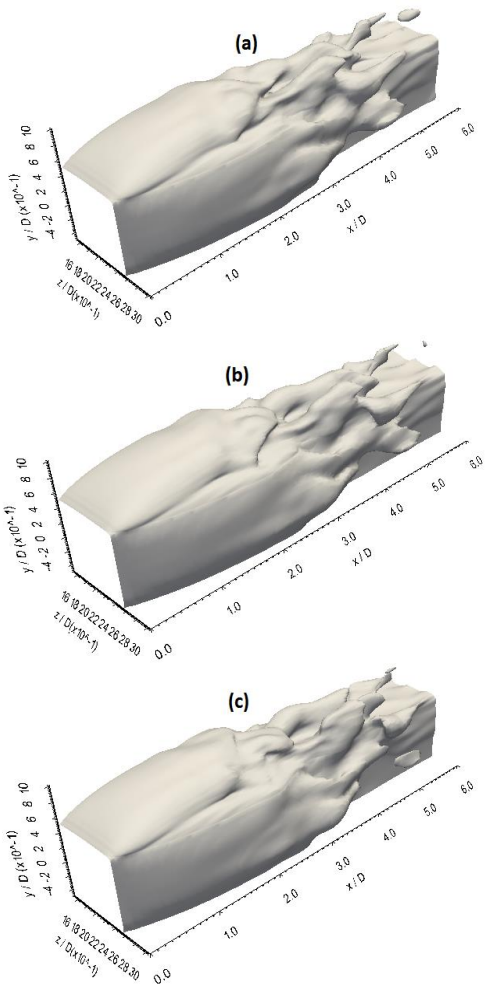

Fig.12 Instantaneous spanwise vorticity on the top and side surfaces at sequential times taken every 250 time steps for the square cylinder

6 Velocity and pressure spectra

In order to elucidate if any type of the three frequency modes may exist in the current study, extensive data of instantaneous velocity components and pressure are calculated at 108 points for the flat plate and 96 points for the square cylinder. Time traces of instantaneous velocity components and pressure are stored at 9 streamwise locations for the flat plate and at 8 streamwise locations for the square cylinder. For the flat plate, streamwise locations include a point just after separation at x/D = 0.25; 5 points are distributed within the mean separation bubble length at x/D = 1, 2, 3, 4, and 5; at the reattachment x/D = 6; and in the developing boundary layer after reattachment x/D = 6.5 and 18. For the square cylinder, streamwise locations are x/D = 0.25 as a point just after separation; x/D = 1, 2, 2.5, and 3 as pointes are distributed within the mean separation bubble length; at the reattachment x/D = 3.4; and in the developing boundary layer after reattachment x/D = 4 and 18.

Instantaneous velocity components and pressure are stored also at three spanwise positions and four wall normal locations for each streamwise location. The spanwise positions are z/D = 1, 2, and 3 for the flat plate and z/D = 1.6, 2, and 2.4 for the square cylinder. For both geometries, the four wall normal locations are y/D = 0.55, 0.8, 1, and 1.5.

For both geometries, a total of 40,000 samples at each point taken every 10 time steps with time step = 2×10^{-6} seconds are collected. This corresponds to a total simulation time of 0.8 seconds. The sampling frequency = 50 kHz. The maximum frequency which can be resolved is about 25 kHz and the lowest is about 1.25 Hz employing the Fourier transform method to process the data. It is worth pointing out that the inspection of the spectra for any instantaneous variable at any spanwise position for the same streamwise and wall-normal locations shows that results are very similar. So, all of the figures which follow correspond to data at the spanwise position is at the center of the computational domain z/D = 2.

For the flat plat, the spectra for the streamwise and wall normal velocities at a point which is close to the separation line and very close to the plate surface (x/D = 0.25, y/D = 0.55) are shown in Fig. 13. At this position, there is no any spectacular high or low frequency peak can be distinguished. At the same streamwise position and at the second wall normal location y/D = 0.8, the pressure spectrum is similar to those in Fig. 13 with no recognised high or low frequency peak as shown in Fig. 14. At this position, the spectra for the streamwise and wall normal velocities (not shown here) do not show any high or low frequency peak. At the same streamwise station and for other two wall normal locations y/D = 1 and y/D = 1.5, the appearance of high or low frequency is not distinguished in the spectra for the velocity components and pressure (not shown here).

At the second stramwise position x/D = 1 and for all wall normal locations, the velocity components and pressure spectra do not present any high or low frequency peak as shown in Fig. 15 for the pressure spectrum at y/D = 0.8, streamwise velocity spectrum

at y/D = 1, and wall normal velocity spectrum at y/D = 1.5.

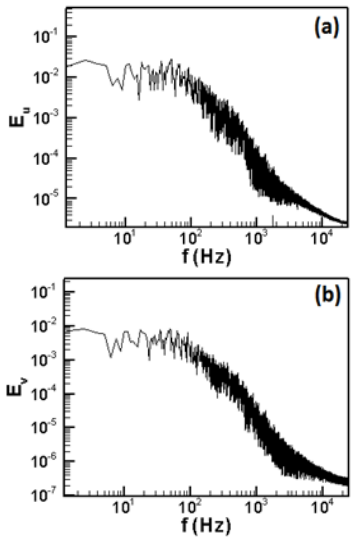

Fig.13 Spectra at x/D = 0.25 and y/D = 0.55 for: (a) streamwise velocity, (b) wall normal velocity for the flat plate

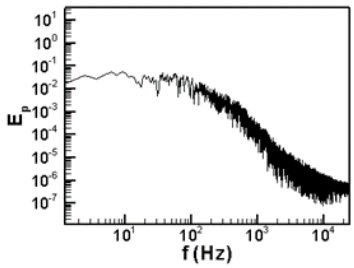

Fig.14 Pressure spectra at x/D = 0.25 and y/D = 0.8 for the flat plate

Moving downstream at the location x/D = 2, the spectra for the velocity components and pressure very close to the plate wall y/D = 0.55 are shown in Fig. 16. In this figure, a peak at the frequency band (approximately 120-140 Hz) is clearly shown. In the current study, this is equivalent to 0.76-0.89 U_0/x_R. At the same streamwise location, moving upward to the wall normal position y/D = 0.8, similar peak of the high frequency band is presented by the spectra for the velocity components and pressure as shown in Fig. 17. At the same streamwise station, moving further along the wall normal axis to the locations y/D = 1 and y/D = 1.5, the velocity components and pressure spectra (not shown here) show similar high frequency band peak 0.76-0.89 U_0/x_R.

This frequency is the characteristic (regular) shedding frequency that is attributed to the shedding of large scale structures from the separation bubble. The current value of this frequency is in a good agreement with values which documented in the literature. For a blunt flat plate with a turbulent separated-reattached flow, the regular shedding frequency which reported in the experimental work of Kiya and Sasaki [6] was 0.6-0.8 U_0/x_R. Cherry et al. [7] observed 0.7 U_0/x_R as the regular shedding frequency. For similar geometry but with a transitional separated-reattached flow, 0.7-0.875 U_0/x_R obtained as the regular shedding frequency in [10]. For such flow on a flat plate with a semicircular leading edge, Yang and Voke [15] revealed 0.77 U_0/x_R as the value of the regular shedding frequency. In a turbulent separated-reattached on different geometries, the regular shedding frequency for a backward-facing step documented as 0.5-0.8 U_0/x_R in [50], 0.6 U_0/x_R in [51], 0.5 U_0/x_R in [11], and 1 U_0/x_R in [52] and [53]. In a long splitter plate, the value of the regular shedding frequency was presented as 0.6-0.9 U_0/x_R in experimental work in [13].

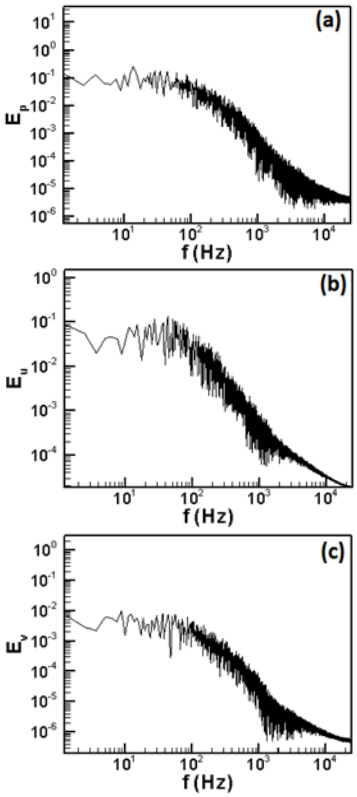

Fig.15 Spectra at x/D = 1 for: (a) pressure at y/D = 0.8, (b) streamwise velocity at y/D = 1, (c) wall normal velocity at y/D = 1.5 for the flat plate

At the center of the separation bubble length x/D = 3 for y/D = 0.55, y/D = 0.8, and y/D = 1.5, the spectra for the velocity components and pressure (not shown here) reveal the regular shedding frequency band 0.76-0.89 U_0/x_R. This frequency is clearly shown in the velocity components and pressure spectra at the same streamwise position for y/D = 1 as shown in Fig. 18.

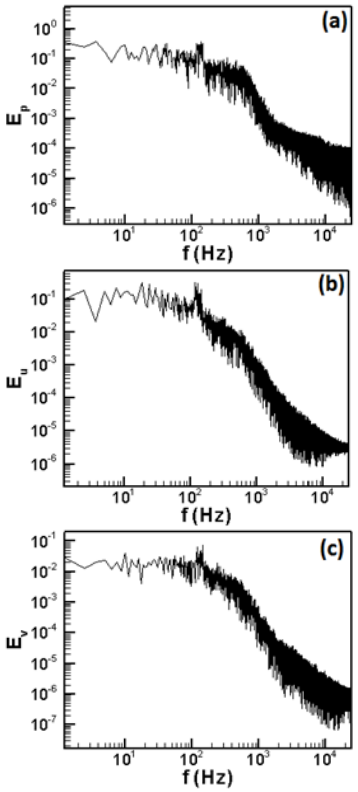

Fig.16 Spectra at x/D = 2 and y/D = 0.55 for: (a) pressure, (b) streamwise velocity, (c) wall normal velocity for the flat plate

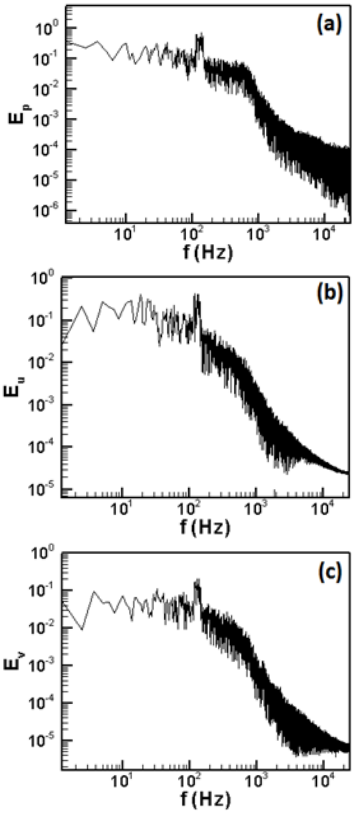

Fig.17 Spectra at x/D = 2 and y/D = 0.8 for: (a) pressure, (b) streamwise velocity, (c) wall normal velocity for the flat plate

Moving downstream to the location x/D = 4, the spectra for the velocity components and pressure very close to the plate surface at y/D = 0.55 are shown in Fig. 19. In this figure, the regular shedding frequency band 0.76-0.89 U_0/x_R is barely shown in the pressure spectra while the velocity components spectra do not show any high or low frequency peak. At same streamwise station, moving upward to all other wall normal locations, the velocity components and pressure spectra (not shown here) do not show any high or low frequency peak. At the streamwise position x/D = 5 and for all wall normal locations, there is no present high or low frequency peak in the velocity components and pressure spectra (not shown here).

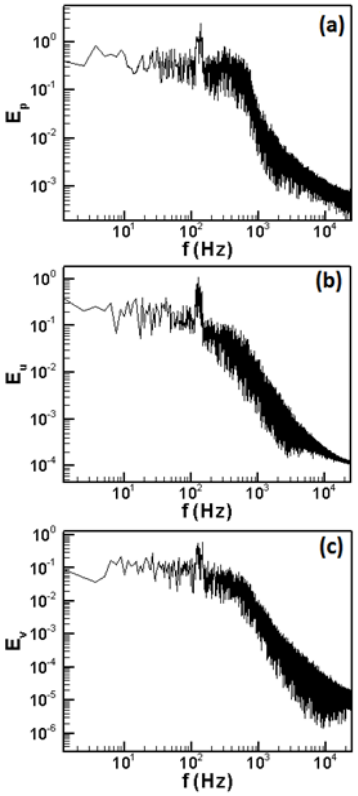

Fig.18 Spectra at x/D = 3 and y/D = 1 for: (a) pressure, (b) streamwise velocity, (c) wall normal velocity for the flat plate

At the reattachment point x/D = 6, the spectra for the velocity components and pressure at y/D = 0.55 are shown in Fig. 20. No high or low frequency peak can be detected in this figure. At all locations further upward for the same streamwise position, there is no noticeable high or low frequency peak in velocity components and pressure spectra (not shown here). Seam scenario of this streamwise location is repeated at the two streamwise points in the turbulent boundary layer x/D = 6.5 and x/D = 18

for all wall normal locations where there is no appearance of high or low frequency peak at those locations. This shown in the spectra for the velocity components and pressure in Fig. 21 for the location x/D = 6.5, y/D = 0.8 and in Fig. 22 for the location x/D = 18, y/D = 1.

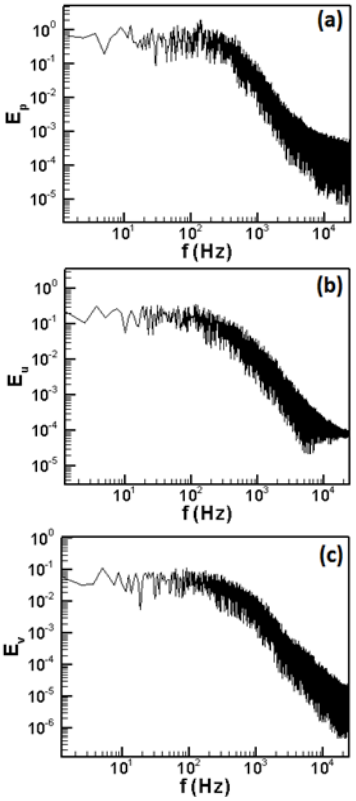

Fig.19 Spectra at x/D = 4 and y/D = 0.55 for: (a) pressure, (b) streamwise velocity, (c) wall normal velocity for the flat plate

For the square cylinder and at the streamwise station x/D = 0.25 which is close to the separation line, the pressure spectrum at y/D = 0.55, streamwise velocity spectrum at y/D = 0.8, and wall normal velocity spectrum at y/D = 1 are shown in Fig. 23. There is no distinguished high or low frequency peak can be observed in these spectra. At the same streamwise position and for all wall normal locations, the other velocity components and pressure spectra (not shown here) do not present a sign of any existing high or low frequency peak.

Moving downstream to the location x/D = 1, the spectra for the velocity components and pressure at y/D = 0.8 are shown in Fig. 24. In these spectra and the spectra at all other wall normal positions (not shown here) at this streamwise station, no obvious high or low frequency peak can be identified.

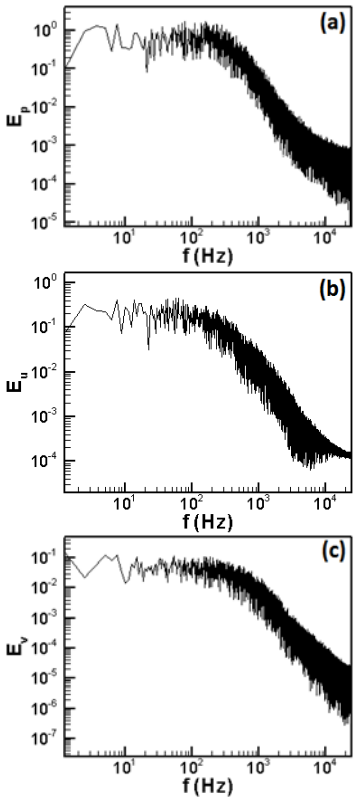

Fig.20 Spectra at x/D = 6 and y/D = 0.55 for: (a) pressure, (b) streamwise velocity, (c) wall normal velocity for the flat plate

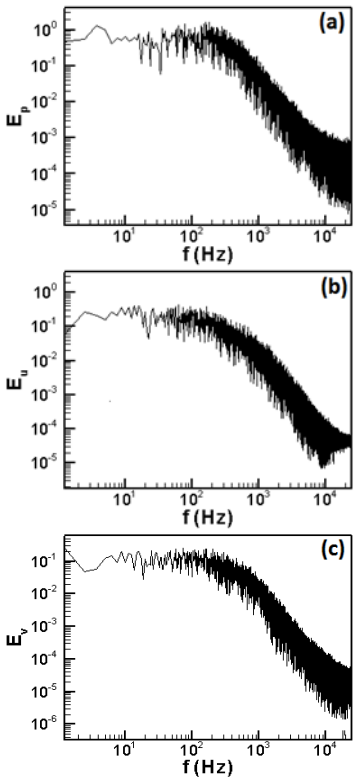

Fig.21 Spectra at x/D = 6.5 and y/D = 0.8 for: (a) pressure, (b) streamwise velocity, (c) wall normal velocity for the flat plate

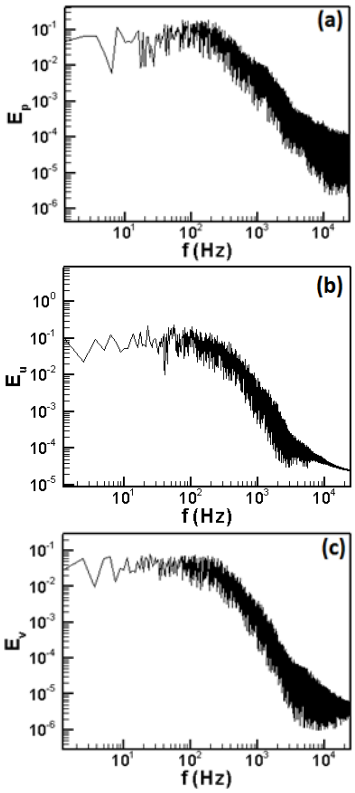

Fig.22 Spectra at x/D = 18 and y/D = 1 for: (a) pressure, (b) streamwise velocity, (c) wall normal velocity for the flat plate

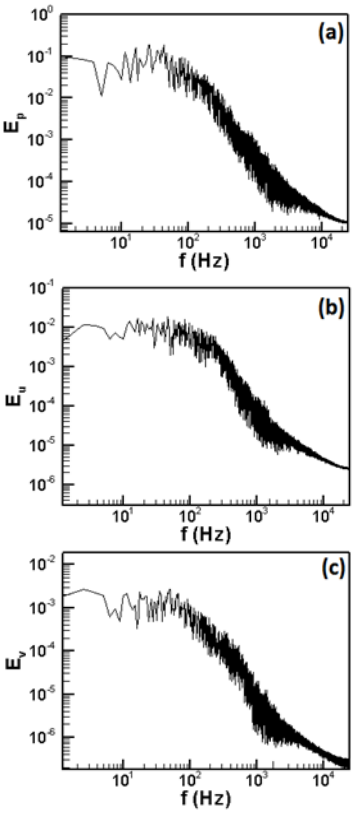

Fig.23 Spectra at x/D = 0.25 for: (a) pressure at y/D = 0.55, (b) streamwise velocity at y/D = 0.8, (c) wall normal velocity at y/D = 1 for the square cylinder

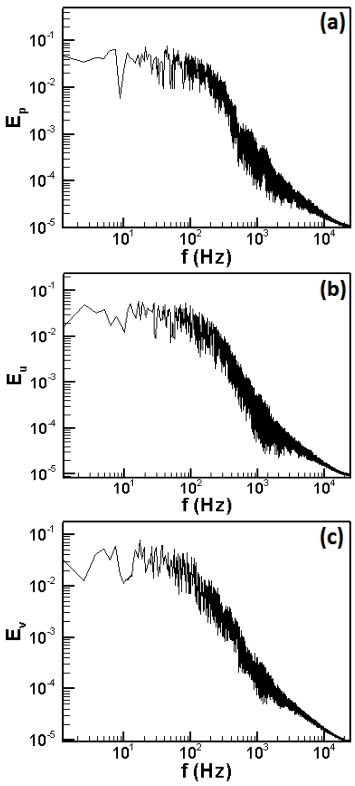

Fig.24 Spectra at x/D = 1 and y/D = 0.8 for: (a) pressure, (b) streamwise velocity, (c) wall normal velocity for the square cylinder

At the streamwise station x/D = 2 and for y/D = 0.8 and y/D = 1 positions, the velocity components and pressure spectra present clearly that there is band of peak frequencies at about 150-180 Hz as shown in Figs. 25 and 26 respectively. In the current study, this is equivalent to $0.54\text{-}0.65U_0/x_R$. This frequency is the characteristic (regular) shedding frequency that is referred to the shedding of large scale structures from the separation bubble. The value of the current regular shedding frequency for the square cylinder is different from that identified for the flat plate. However, the current regular shedding frequency for the square cylinder is close to the regular shedding frequencies in other studies which presented in the flat plate case. The velocity components and pressure spectra (not shown here) at wall normal locations y/D = 0.55 and y/D = 1.5 at same streamwise position show same value of the regular sheading frequency band $0.54\text{-}0.65U_0/x_R$.

For all wall normal locations at the streamwise position x/D = 2.5, the spectra for the velocity components and pressure present clearly the existence of the regular shedding frequency band $0.54\text{-}0.65U_0/x_R$. This shown in Fig. 27 at the wall normal position y/D = 0.8. Going further downstream at x/D = 3, the regular shedding frequency band $0.54\text{-}0.65U_0/x_R$ can hardly be identified in the velocity components and pressure

spectra at just the first and second wall normal positions y/D = 0.55 and y/D = 0.8 where there is no appearance of this frequency peak at other wall normal locations. This clearly shown in Fig. 28 for the streamwise velocity spectrum at this streamwise location for all wall normal positions.

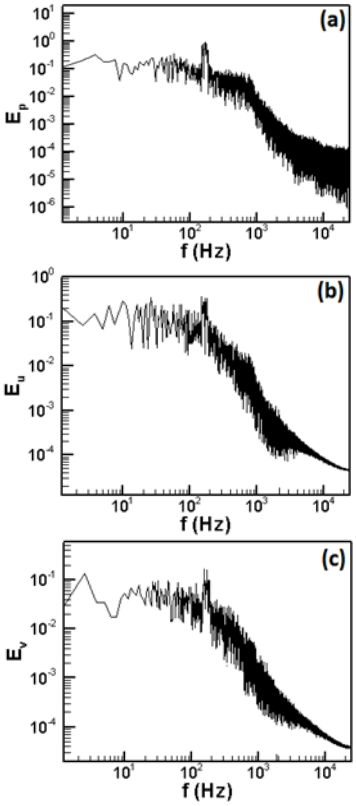

Fig.25 Spectra at x/D = 2 and y/D = 0.8 for: (a) pressure, (b) streamwise velocity, (c) wall normal velocity for the square cylinder

At the reattachment x/D = 3.4 for all wall normal locations, there is no sign of any apparent high or low frequency peak in the velocity components and pressure spectra as shown in the Fig. 29 for the wall normal location y/D = 0.8. No high or low frequency peak can be observed in the velocity components and pressure spectra at all wall normal positions for the two streamwise points which located in the turbulent boundary layer. This shown in Figs. 30 and 31 for points coordinates x/D = 4, y/D = 0.55 and x/D = 18, y/D = 0.8 respectively.

For both geometries, there is no any trace of the selective high frequency mode or low frequency mode (shear layer flapping) in the thorough spectra analysis for the velocity components and pressure in the current study.

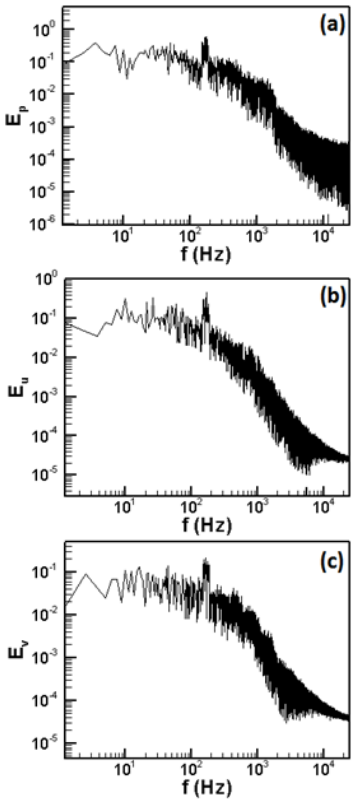

Fig.26 Spectra at x/D = 2 and y/D = 1 for: (a) pressure, (b) streamwise velocity, (c) wall normal velocity for the square cylinder

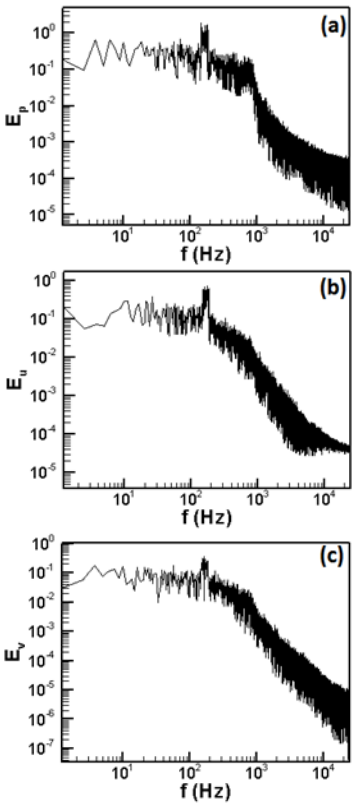

Fig.27 Spectra at x/D = 2.5 and y/D = 0.8 for: (a) pressure, (b) streamwise velocity, (c) wall normal velocity for the square cylinder

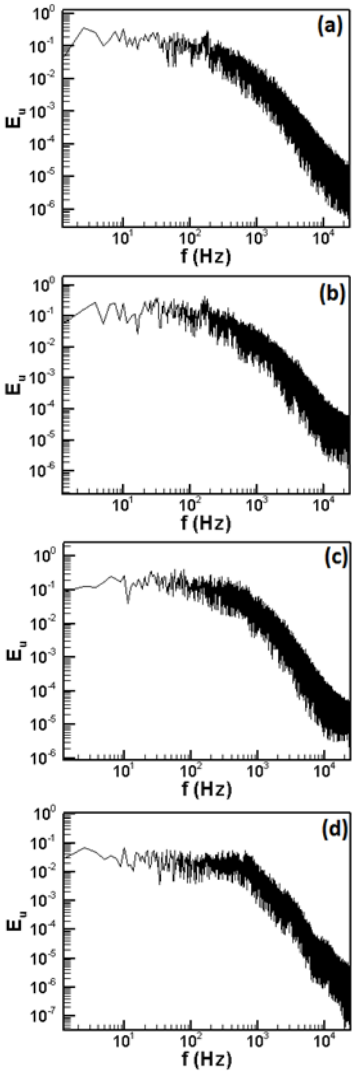

Fig.28 Streamwise velocity pectra at x/D = 3 and: (a) y/D = 0.55, (b) y/D = 0.8, (c) y/D = 1, (d) y/D = 1.5, for the square cylinder

The selective high shedding frequency mode detected in [8] for turbulent separated-reattached flow and in [10] for transitional separated reattached flow over a blunt flat plate. In these studies, the value of this high shedding frequency estimated to be seven times of the regular shedding frequency. If the selective high shedding frequency exists in the current study, its value will be of the order 5.32-6.23 U_0/x_R for the flat plate and 3.78-4.55 U_0/x_R for the square cylinder. This is equivalent to 836-979 Hz for the flat plate and 1048-1261 Hz for the square cylinder. So, the selective high shedding frequency would happen every 0.0012-0.001 (the average = 0.0011) seconds for the flat plate and 0.0009-0.0007 (the average = 0.0008) seconds for the square cylinder if it exists. In the current study, the samples collected time is 0.8 seconds can cover 827 and 1000 cycles approximately of the selective high shedding frequency if it exists in the flat plate and square cylinder respectively.

However, the high frequency mode noticed in experimental work of turbulent separation in [6] for a blunt flat plate and in [11] for a backward-facing step. Therefore, we suggest that the high frequency mode may be an integral feature of turbulent separation flows and it is not present in the case of transitional separated-reattached flows.

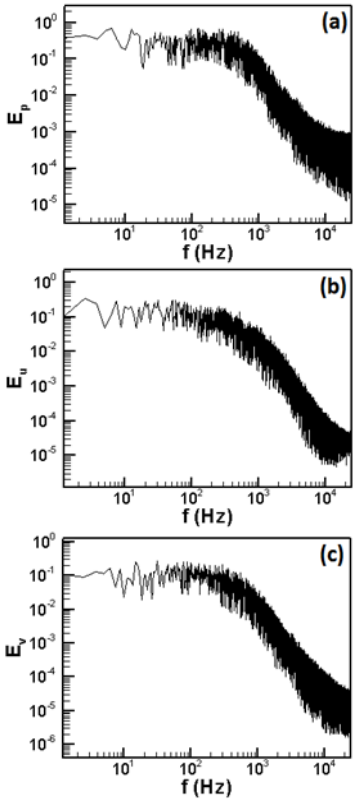

Fig.29 Spectra at x/D = 3.4 and y/D = 0.8 for: (a) pressure, (b) streamwise velocity, (c) wall normal velocity for the square cylinder

The low frequency mode (low frequency flapping) that is believed to be due to the free shear layer flapping has identified in many turbulent separation studies and just in transitional separated-reattached flow in [15]. Hillier and Cherry [9], Kiya and Sasaki [6], and Cherry et al. [7] detected this low frequency value to be of the order $0.12U_0/x_R$. Based on the current data, this is equivalent to 18.85 Hz in the flat plate and 33.26 Hz in the square cylinder. So, the low frequency flapping would happen every 0.05 sec for the flat plate and 0.03 sec for the square cylinder if it exists. In the current study, the sampling is carried out over 0.8 seconds for both geometries. So, the current samples are able to cover 16 and 27 low frequency cycles if it exists in the flat plate and square cylinder respectively. It is worth pointing out that the sampling time in Tafti

and Vanka [8] was equivalent to just three low frequency cycles and this phenomenon was captured in this study.

We believe that the reason of disappearing the low frequency flapping is due to the action of the laminar part of the separation bubble which works as a filter to filter this low wavenumber motion of the shear layer as suggested by Abdalla and Yang [10]. In addition, this phenomenon may only appear in turbulent separated-reattached flows as suggested by Cherry et al. [7].

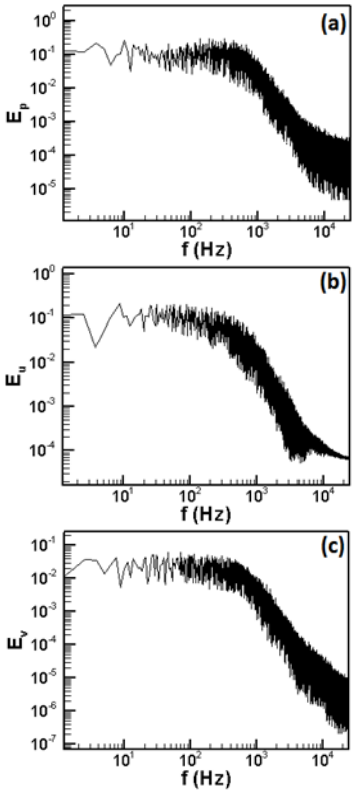

Fig.30 Spectra at x/D = 4 and y/D = 0.55 for: (a) pressure, (b) streamwise velocity, (c) wall normal velocity for the square cylinder

7 Coherent structures

To have an initial conception for formation and development of the vortices, x-y plane of pressure contours at sequential times (every 250 time steps) at the mid-distance of spanwise direction z/D=2 are shown in Figs. 32 and 33 for the flat plate and square cylinder respectively. In the flat plate case, it can be observed that the weak vortices start to construct at about x/D=1.8 and move along the edge of the separated shear layer. They become larger and stronger by merging with each other as they move downstream in the region about x/D = 3 to 4, where a considerable three-dimensional motion takes place. Around the reattachment location at x/D = 6, the large structure breaks down to a group of small structures which shed to the turbulent boundary layer as shown in Figs. 32(e) and 32(f). In the meantime, there is a construction of another structures and they move from upstream where there is a repetition of the above scenario.

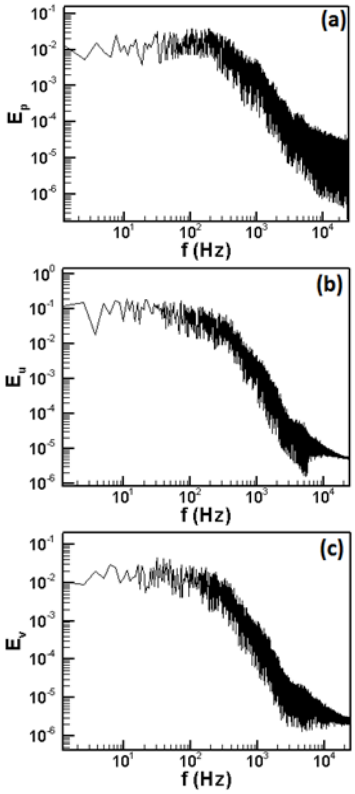

Fig.31 Spectra at x/D = 18 and y/D = 0.8 for: (a) pressure, (b) streamwise velocity, (c) wall normal velocity for the square cylinder

In the square cylinder case, it can be seen that the Kelvin-Helmholtz rolls are formed and shed at the separated layer at about x/D = 1.8. These rolls disintegrate to small structures within the turbulent flow downstream of the reattachment zone. It can be seen there is no vortices merging process in this case as that is shown in the flat plate case. The distance of vortical structure development is shorter and the separation bubble is smaller in the square cylinder case. In this geometry, it can be clearly observed that there is a periodic process of forming, moving, disintegrating, and shedding of the structures as shown in Fig. 33.

The fact that no vortices merges in the square cylinder is most likely due to the twisting nature of the Kelvin-Helmholtz structure. This may lead to early breaking down of this coherent structure to four Kelvin-Helmholtz structures on each surface. This event may reduce the ability of Kelvin-Helmholtz structures to merge with each other.

Thus, it can be concluded that the transition stages in the square cylinder are shorter in the space and time than the transition stages in the flat plate. The transition to the turbulence in the square cylinder takes place faster to form a small separation bubble compared with the separation bubble that constructed in the flat plate.

For more accurate realization of coherent structures formation, a three-dimensional visualization of coherent structures is employed here using flow visualization methods that include low pressure isosurface, vorticity fields isosurface and Q-criterion isosurface.

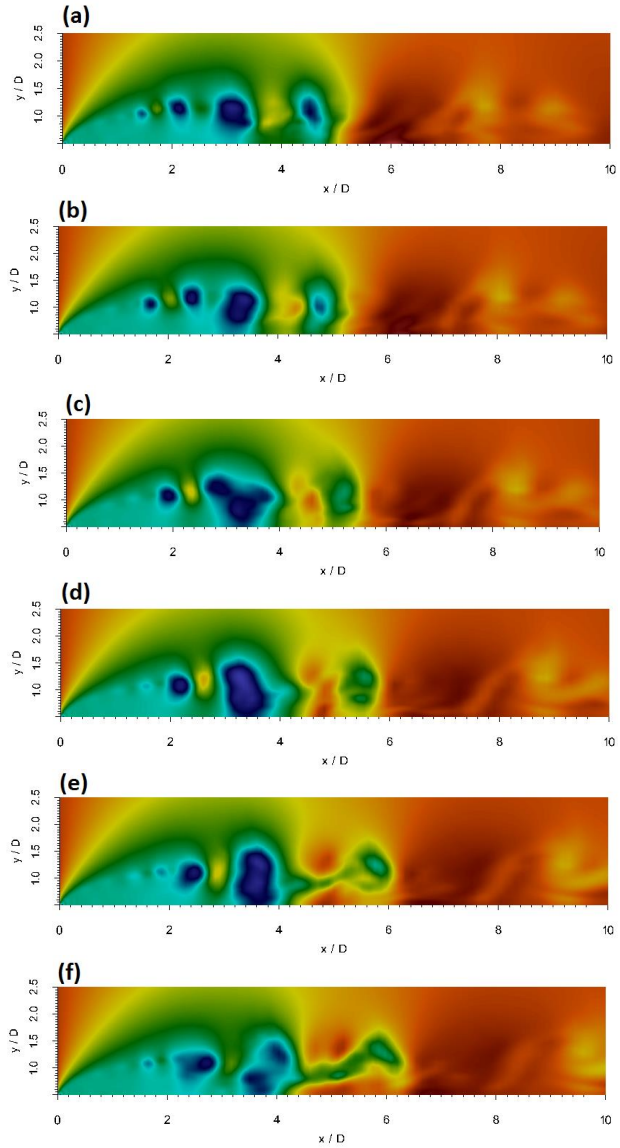

Fig.32 x-y plane of instantaneous pressure contour for the flat plate displaying vortex formation and shedding at sequential times taken every 250 time steps

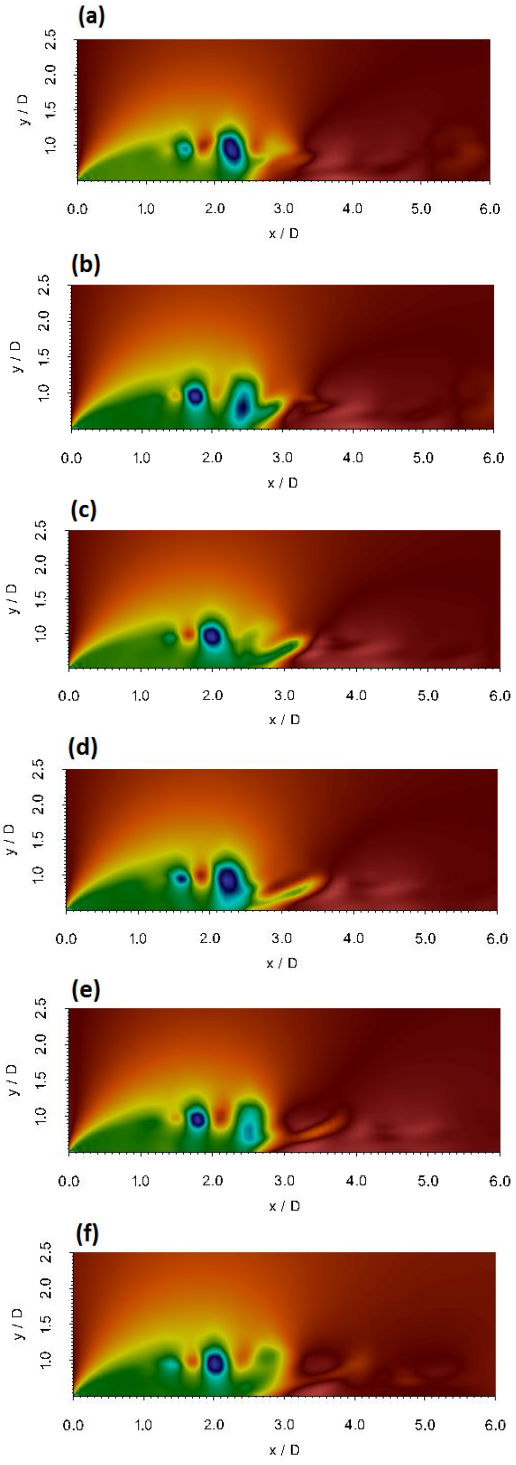

Fig.33 x-y plane of instantaneous pressure contour for the square cylinder displaying vortex formation and shedding at sequential times taken every 250 time steps

7.1 Low pressure isosurface

In the current study, low fluctuating pressure isosurface is adopted as one of the flow visualization schemes. Four low fluctuating pressure isosurfaces for the flat plate taken at sequential times every 250 time steps are shown in Fig. 34.

Flow topology presents a shedding of two-dimensional Kelvin-Helmholtz rolls downstream of the plate leading edge, which grow in size while moving downstream as shown in Fig. 34(a). It is clearly shown that this growth is due to merging between two rolls as shown in Fig. 34(c) where there are two Kelvin-Helmholtz structures catch up with each other and merge to form one large structure. This big vortex is not two-dimensional in nature and breaks down into small three-dimensional hairpin structures around the reattachment region. Inspection of the flow topology for extensive data at more time steps shows a similar but not exact scenario of the flow topology that shown in Fig. 34.

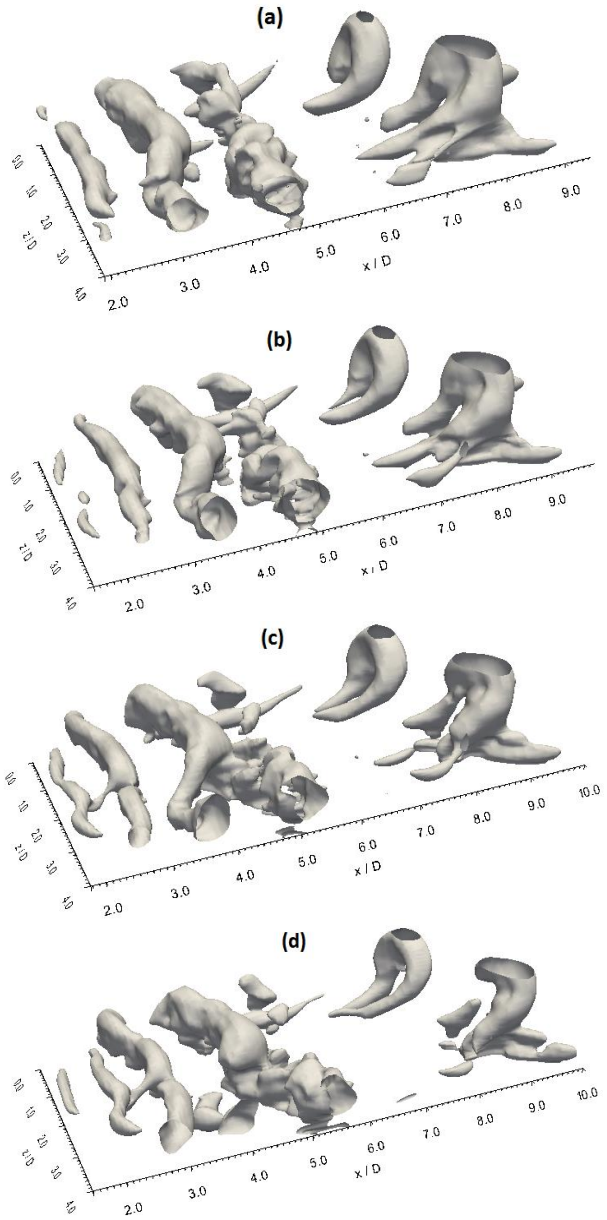

Fig.34 Low pressure isosurface at sequential times taken every 250 time steps for the flat plate

Abdalla and Yang [40] reported that the new structure that formed from the merging of Kelvin-Helmholtz rolls process stretched in the streamwise direction and evolved into hairpin and rib-like structures due to the helical instability effect, which was considered as a secondary instability mechanism. They reported that the longitudinal structures were as braids between consecutive Kelvin-Helmholtz rolls i.e., there were interactions between spanwise and streamwise vortices. Despite forming a large structure from merging two Kelvin-Helmholtz rolls and breaking down this structure into hairpin structures in the current study, the current secondary instability mechanism is different, because there is no any stretching of the vortical structures, and the small three-dimensional structures are not a result of a topological evolution of the large two-dimensional structures. Existence of the small structures is due to a direct breaking down of the large structures. It should be noted that rib-like structures are not formed here.

Direct disintegration of the large structure was reported for different geometrical shapes for the transitional separated-reattached flow. In cases of a surface mounted obstacle and forward-facing step, Abdalla et al. [41] observed this phenomenon. They reported that the secondary instability was different from the helical instability mechanism. Direct breaking down of the large structure in to hairpin structures was shown in their flow visualisation. Rib-like structures were also not recognised in their study. This may confirm our secondary instability mechanism of forming the three-dimensional structures, which is different from the helical instability mechanism.

Low fluctuating pressure isosurfaces for the square cylinder taken every 250 time steps are shown in Fig. 35. It can be seen Kelvin-Helmholtz rolls are formed at about x/D=1.8. They move and become larger in size when convecting downstream of the leading edge. As mentioned in the x-y plane of pressure contours shown in Fig. 33, there is no merging of the vortices in this case. The large Kelvin-Helmholtz structure develops topologically to become a hairpin structure between x/D=3 and x/D=3.5. At the further downstream, it is clearly shown that the hairpin structures shed to the turbulent attached flow and disintegrate to the smaller structures.

The low pressure isosurface in the square cylinder confirms that there is no vortices merging process in this geometry as one of the transition events and presents that the forming of the hairpin structures is due to a topological evolution of the Kelvin-Helmholtz rolls. The low pressure isosurface

of the flat plate shows a large structure forming from a pairing of two Kelvin-Helmholtz rolls, then such a large structure breaks down in to many hairpin structures.

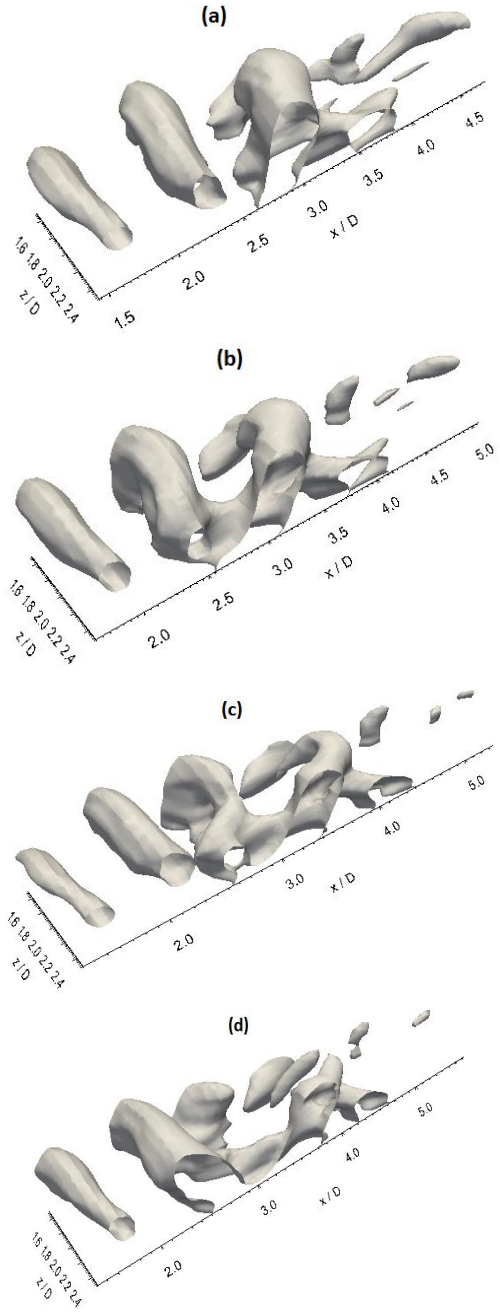

Fig.35 Low pressure isosurface at sequential times taken every 250 time steps for the square cylinder

7.2 Vorticity fields isosurface

Vorticity magnitude is one of many parameters which conventionally used to visualize the flow field. Vorticity magnitude isosurfaces for the flat plate and square cylinder are shown in Figs. 36 and 37 respectively. For both geometries, three isosurfaces for vorticity magnitude are taken at three sequential times (every 250 time steps). There is a plane sheet of the vorticity at the laminar region of the flow between the leading edge and the location of the onset of the flow unsteadiness at about x/D=1.8 for both geometries as shown in Figs. 36 and 37. After this region, three-dimensional hairpin structures are formed associated with a three-dimensionality nature of the flow. For both geometries, the vorticity field shows a three-dimensional turbulent flow in the high shear turbulent region after the reattachment zone.

In the square cylinder, the vorticity magnitude isosurfaces for the top and side surfaces at three sequential times (every 250 time steps) are shown in Fig. 38. It is clearly seen that there is no difference in vorticity development on both surfaces. Two plane sheets of the vorticity on each surface develop to be hairpin structures that break down to small structures within the turbulent flow after the reattachment.

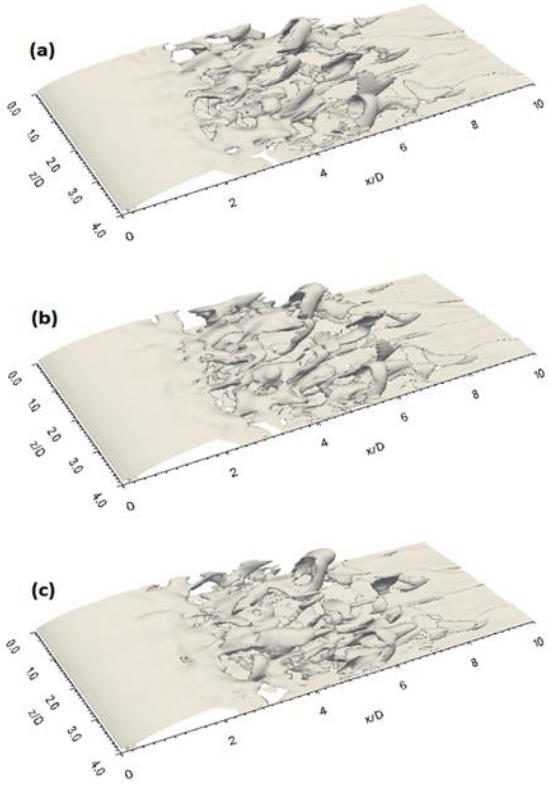

Fig.36 Vorticity magnitude isosurface at sequential times taken every 250 time steps for the flat plate

As shown in Figs. 36-38, the vorticity magnitude isosurface shows just small hairpin structures of the flow clearly while the transition events such as construction of Kelvin-Helmholtz rolls and their pairing process in the flat plate or their evolution in the square cylinder are not shown by this technique. So, all types of existent coherent structures cannot be described by vorticity magnitude isosurface.

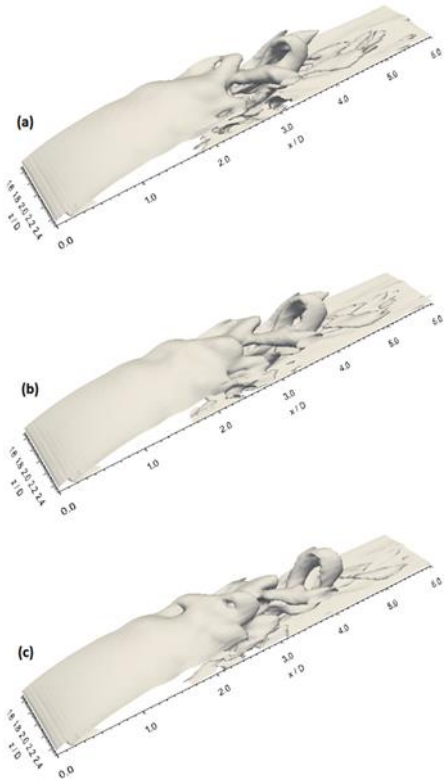

Fig.37 Vorticity magnitude isosurface at sequential times taken every 250 time steps for the square cylinder

Streamwise vorticity isosurface for the flat plate and square cylinder are shown in Figs. 39 and 40 respectively. There is no trace of streamwise vorticity before the location of x/D=1.8 for both geometries. After this location, the streamwise vorticity is developed from x/D = 4 to x/D = 6 in the flat plate as shown in Fig. 39. It can be seen an existence of the streamwise vortical structures at the turbulent boundary layer after the reattachment region and they travel a distance before disintegrating to smaller structures. It is clearly shown that the streamwise vortical structures have an angle with the solid wall (lifted up) and this angle may be the reason of existence of these structures after the reattachment region. The streamwise vorticity for the square cylinder is shown in Fig. 40, presents a same scenario of that identified in Fig. 39 but with a faster disintegration of the vortical structures in the turbulent boundary layer.

Inspection of wall normal vorticity refers to existing similar inclined structures that identified in previous two figures for both geometrical shapes. This is shown in Fig. 41 for the flat plate and Fig. 42 for the square cylinder. It is clearly seen that the disintegration of the vortical structures takes place in the square cylinder faster than that in the flat plate. Similar behavior is observed in the streamwise vorticity isosurfaces. This behavior of vortical structures can be refered to the recovery of the turbulent boundary layer, which happened much faster in the square cylinder than that in the flat plate.

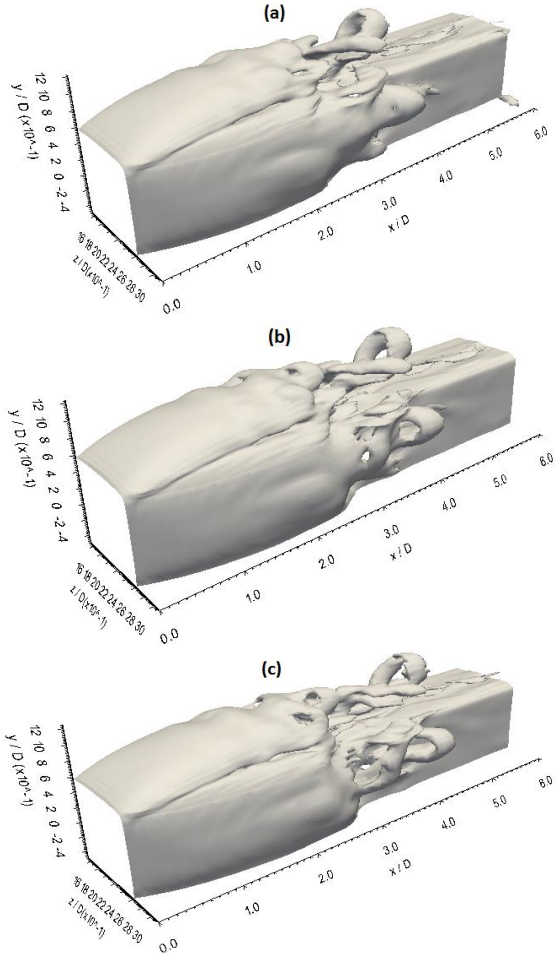

Fig.38 Vorticity magnitude isosurface on the top and side surfaces at sequential times taken every 250 time steps for the square cylinder

Isosurfaces of spanwise vorticity for both geometries are shown in Figs. 43 and 44, in which a plane sheet of vorticity starts from the leading edge is elucidated. For the flat plate, this sheet shows wrinkling as a result of disturbance growing, which indicates to transition starting as shown in Fig. 43. It can be seen that a development of the spanwise vorticity takes place at the region from x/D = 4 to x/D = 6 leading to a formation of longitudinal structures that travel toward to the reattachment zone. At the farther downstream, these structures break down to small structures within the turbulent boundary layer. It can be seen a comparable conduct of the spanwise vorticity for both geometries with just a deference of locations of vorticity development as shown in Figs. 43 and 44.

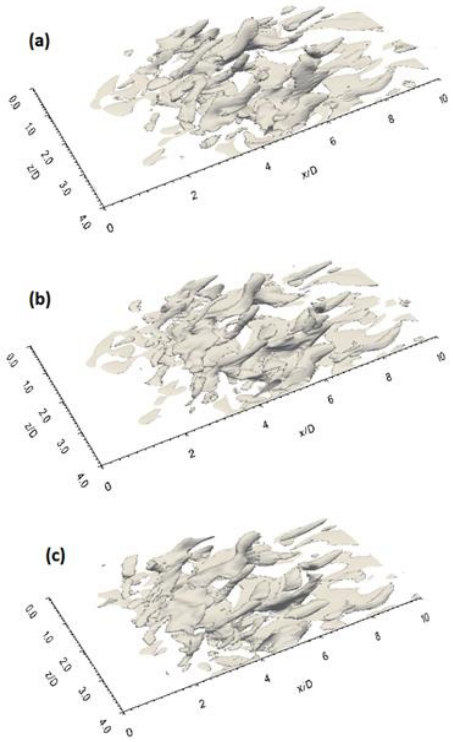

Fig.39 Streamwise vorticity isosurface at sequential times taken every 250 time steps for the flat plate

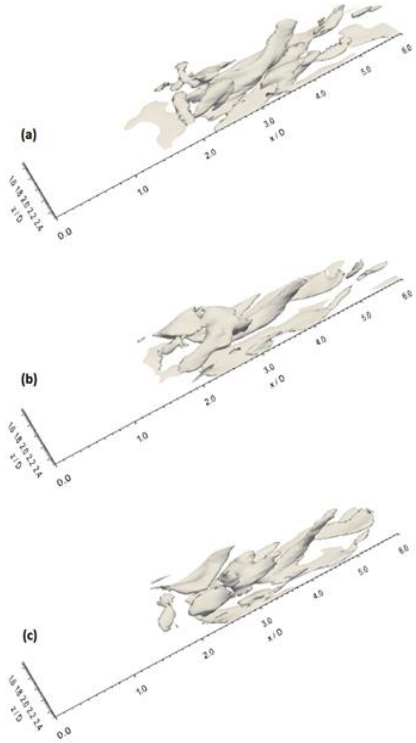

Fig.40 Streamwise vorticity isosurface at sequential times taken every 250 time steps for the square cylinder

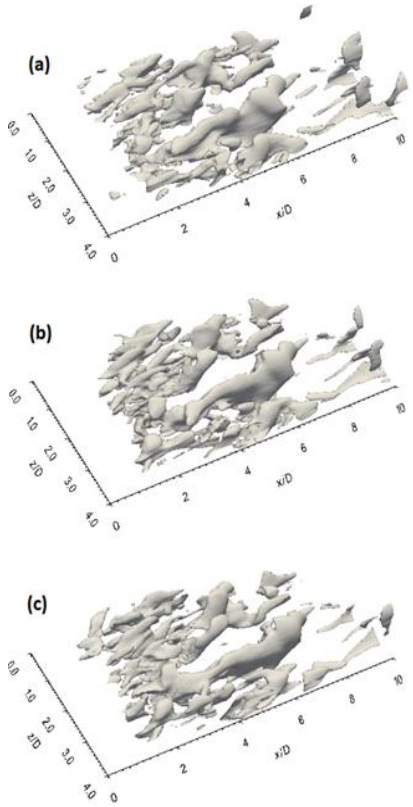

Fig.41 wall normal vorticity isosurface at sequential times taken every 250 time steps for the flat plate

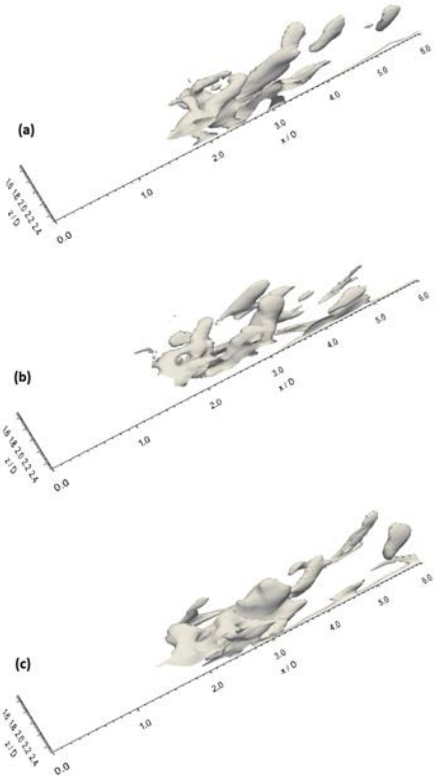

Fig.42 wall normal vorticity isosurface at sequential times taken every 250 time steps for the square cylinder

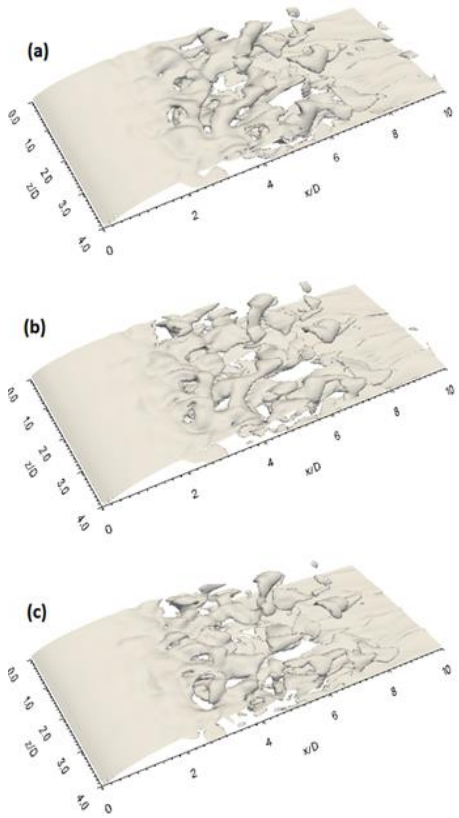

Fig.43 Spanwise vorticity isosurface at sequential times taken every 250 time steps for the flat plate

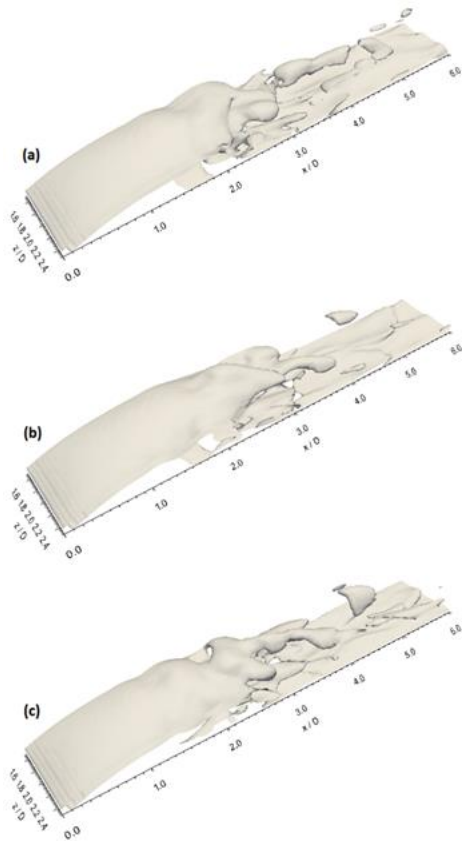

Fig.44 Spanwise vorticity isosurface at sequential times taken every 250 time steps for the square cylinder

For all vorticity components isosurfaces which are shown in Figs. 39-44, it can be concluded that coherent structures of the transition and their evolution are not illustrated clearly by using these flow visualization techniques. This considered as a shortcoming of using these techniques for this purpose.

7.3 Q-criterion isosurface

The flow visualization technique that shares some properties from the vorticity and pressure criterion is called the Q-criterion or second invariant of velocity gradient tenser (Δu) [54]. The Q-criterion is defined as

$$Q = \frac{1}{2}(\Omega_{ij}\Omega_{ij} - S_{ij}S_{ij}) \quad (11)$$

where $(\Omega_{ij}\Omega_{ij})$ is the rotation (vorticity) rate and $(S_{ij}S_{ij})$ is the strain rate where Q-criterion is a balance between them.

The antisymmetric component (Ω_{ij}) of Δu is

$$\Omega_{ij} = \frac{u_{i,j} - u_{j,i}}{2} \quad (12)$$

and the symmetric component (S_{ij}) of Δu is

$$S_{ij} = \frac{u_{i,j} + u_{j,i}}{2} \quad (13)$$

Q-criterion isosurfaces for the flat plate taken at every 250 time steps are shown in Fig. 45. Despite the merging of two Kelvin-Helmholtz rolls process is captured in Figs. 45(a) and 45(b), its clarity is lower than that presented in the low pressure isosurface that shown in Fig. 34. However, the braking down of the new large structure into many small hairpin vortices and their disintegration to smaller structures downstream of the reattachment zone can be seen clearly.

Q-criterion isosurfaces for the square cylinder are presented at every 250 time steps as shown in Fig. 46. It is clearly seen that the Kelvin-Helmholtz rolls are formed and shed from the separated shear layer downstream the leading edge. They move downstream and change to be hairpin structures around the reattachment zone. At the further downstream, hairpin structures shed and disintegrate to smaller turbulent structures in the turbulent attached flow. This is clearly indicated that there is no merging or pairing process of the Kelvin-Helmholtz rolls in this case where each of these rolls develops to form one hairpin structure.

Development of coherent structures of the transition in the top and side surfaces of the square cylinder can be seen in Fig. 47. Q-criterion isousurfaces are taken at three sequential times (every 250 time steps). It is clearly seen that the twisting Kelvin-Helmholtz rolls around this shape

break down in to small Kelvin-Helmholtz rolls on each surface. These rolls are developed topologically to form hairpin structures around the reattachment zone. At the further downstream, three-dimensional hairpin structures shed to the turbulent attached flow and disintegrate into smaller structures. This refers to the similarity of coherent structures behavior on each surface of the square cylinder.

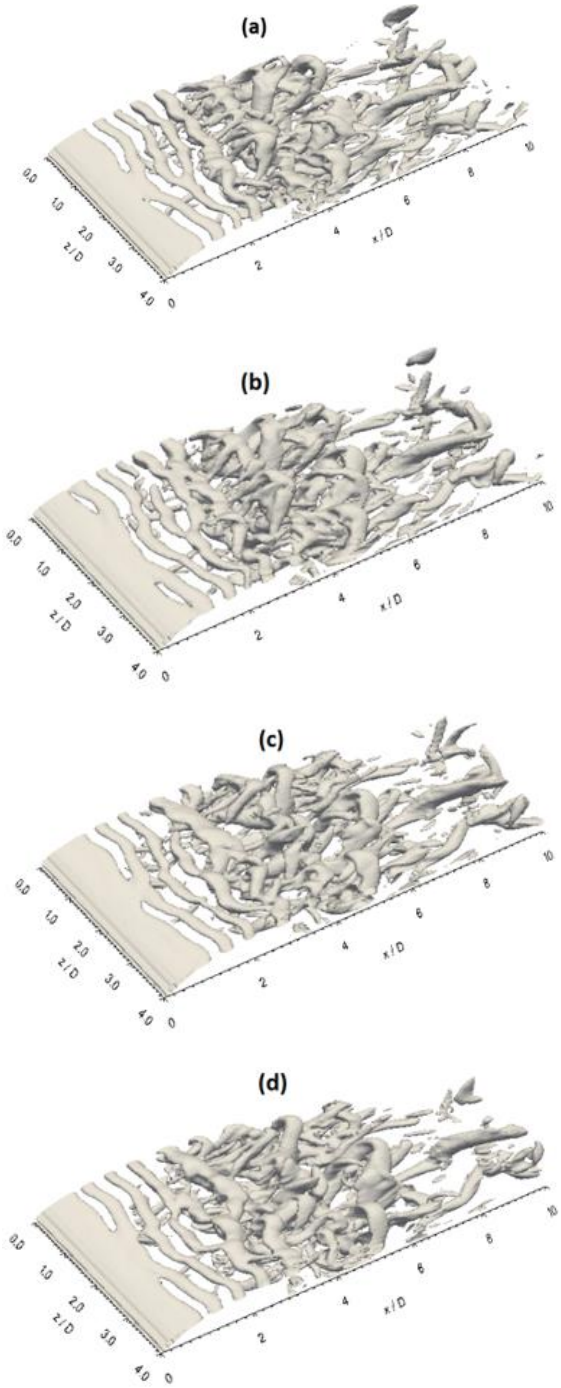

Fig.45 Q-criterion isosurface at sequential times taken every 250 time steps for the flat plate

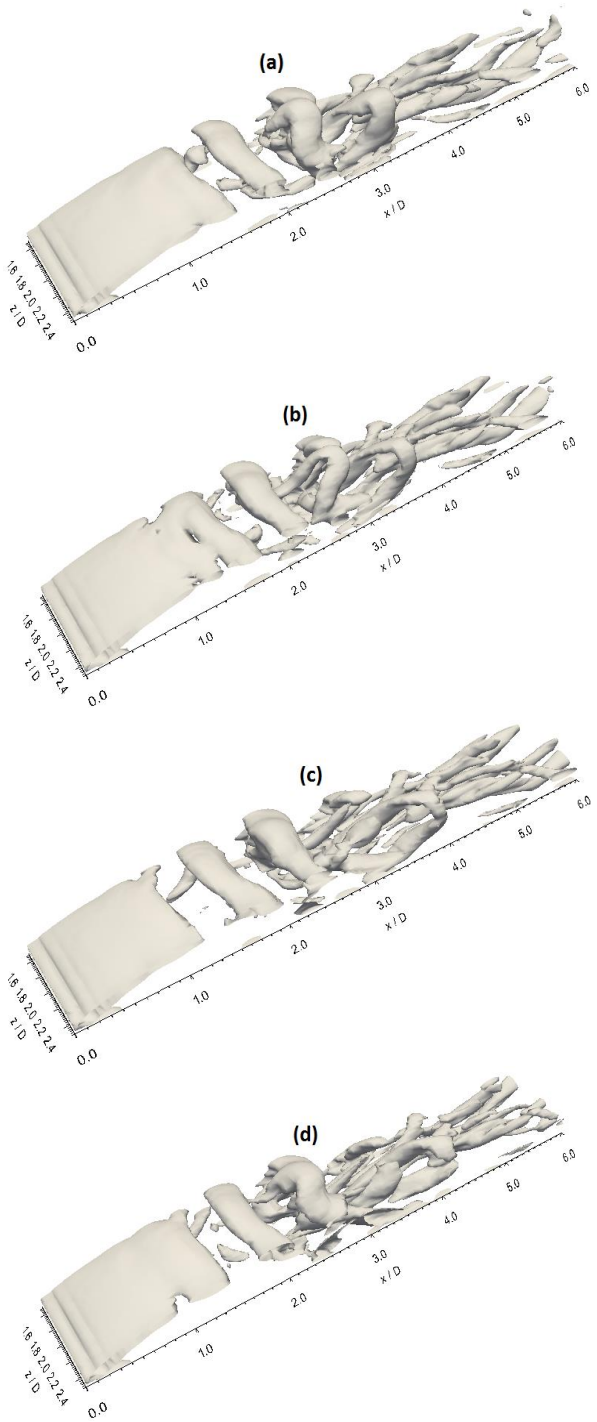

Fig.46 Q-criterion isosurface at sequential times taken every 250 time steps for the square cylinder

It can be observed in the current study that the low pressure isosurface illustrates the large two-dimensional structures better than the small three-dimensional structures. The pairing and merging of two Kelvin-Helmholtz rolls for the flat plate are clearly shown by using this technique. The Q-criterion isosurface is perfect to show the formation of the small hairpin structures and how the Kelvin-

Helmholtz roll develops to a hairpin structure, especially in the square cylinder.

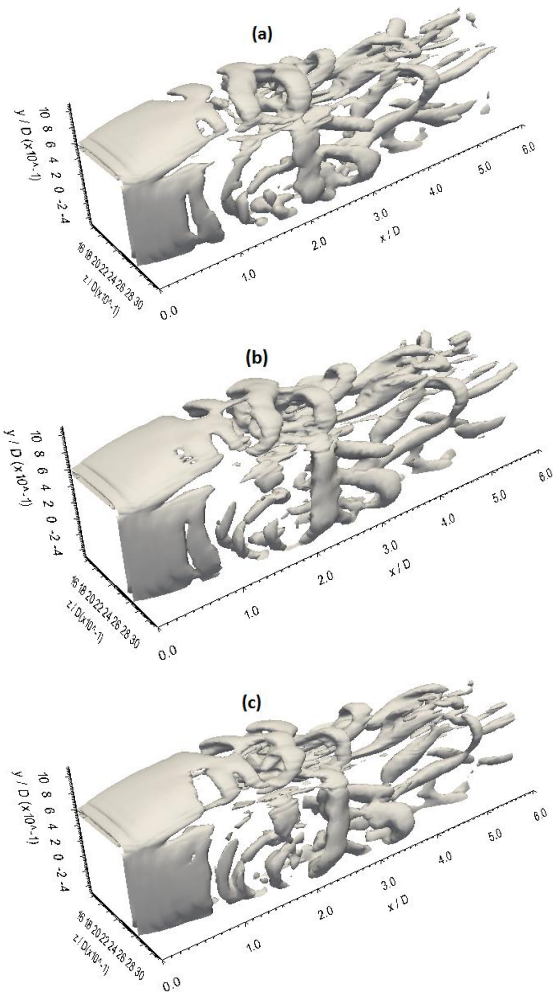

Fig.47 Q-criterion isosurface on the top and side surfaces at sequential times taken every 250 time steps of the square cylinder

8 Conclusions

Aspects of transitional separated-reattached flow have been addressed using data obtained from large eddy simulation by using Open FOAM CFD toolbox. The main purpose of the current study is to shed a light on shedding frequencies and coherent structures evolution of transitional separated-reattached flow on both two-dimensional flat plate with a rectangular leading edge and three-dimensional square cylinder. Results of the flat plate are compared reasonably with available numerical and experimental results. Due to no results of the square cylinder in the literature, its findings are presented for the first time in the present paper. Comparison between the mean values profiles of both geometrical shapes reveals that these profiles bear many aspects of similarities.

The comparisons with the previous experimental and numerical results with present simulated results prove the correctness and feasibility of established numerical simulation methodology for transitional separated-reattached flows by embedding user-defined functions into Open FOAM software.

Based on the current LES data, the value of the characteristic shedding frequency that associated with the shedding of large structures from the free shear layer for the square cylinder is different from that for the flat plate. For both geometries, there is no any trace of the low frequency flapping of the shear layer and selective high frequency.

The low frequency flapping was presented in most experimental and numerical studies for a turbulent separation and in just one transitional separation study that presented by Yang and Voke [15]. Abdalla and Yang [10] showed that the transitional separated-reattached flow did not have this low wavenumber motion due to the laminar part of the separation bubble which filters this low frequency. Their conclusion is further confirmed by the current study regarding this matter. The high selective vortex shedding frequency, which is higher than the regular shedding frequency reported in very few studies with no explanation of the cause of this phenomenon. The current study tries to discover this high frequency if it exists. Absence of this mode leads us to draw the conclusion that the selective high frequency will be apparent just in a turbulent separation case.

Traditional flow visualization method involving isosurfaces of low pressure, velocity magnitude, vorticity fields, and Q-criterion are used here. For both geometrical shapes, there is a resemblance between the present coherent structures. In the early stage of the transition, there two-dimensional Kelvin-Helmholtz rolls are formed downstream of the leading edge. In the square cylinder case, these rolls are twisting around this geometry while they stay flat in the case of the flat plate. Further downstream, these rolls improve to become smaller scale hairpin structures. Finally, hairpin structures shed to the attached turbulent flow and disintegrating into smaller structures.

Despite the existence coherent structures in both geometrical shapes seem to be similar, the flow topology and the mechanism of formation of these structures are different. In the flat plate case, two of Kelvin-Helmholtz rolls merge by pairing around each other to form a large structure. This structure breaks down directly into many hairpin structures around the reattachment zone. In the case of the square cylinder, there is no merging or pairing of the Kelvin-Helmholtz rolls where they evolve

topologically to form hairpin structures around the reattachment location. In this geometry, it is believed that the breaking down of twisting Kelvin-Helmholtz rolls into four small Kelvin-Helmholtz rolls on each surface reduces the ability of the pairing process of vortices. Due to the absence of the pairing process, the transition is shorter and the laminar separation bubble is smaller than that in the flat plate case.

For the square cylinder case, the current study presents the separated shear layer on both up and side surfaces and shows that there is no difference between the coherent structures and the flow topology on each surface.

References:

[1] Taghinia, J., Rahman, M., and Siikonen, T., Large Eddy Simulation of Flow Past a Circular Cylinder with a Novel Sub-Grid Scale Model, European Journal of Mechanics B/Fluids, Vol. 52, 2015, pp. 11-18.X1.

[2] Alving A. E. and Fernholz H. H., Turbulence Measurements around a Mild Separation Bubble and Downstream of Reattachment, *Journal of Fluid Mechanics*, Vol. 322, 1996, pp. 297-328.

[3] Schreck, S. J. and Robinson, M. C., Horizontal Axis Wind Turbine Blade Aerodynamics in Experiments and Modeling, *IEEE Transactions on Energy Conversion*, Vol. 22, No. 1, 2007, pp. 61-70.

[4] Bak, C., Madsen, H. A., Fuglsang, P., and Rasmussen, F., Observations and Hypothesis of Double Stall, *Wind Energy*, Vol. 2, No. 1, 1999, pp. 195-210.

[5] Rist, U. and Augustin, K., Control of Laminar Separation Bubbles Using Instability Waves, *AIAA Journal*, Vol. 44, No. 10, 2006, pp. 2217-2223.

[6] Kiya, M. and Sasaki, K., Structure of a Turbulent Separation Bubble, *Journal of Fluid Mechanics*, Vol. 137, 1983, pp. 83–113.

[7] Cherry, N. J., Hillier, R., and Latour, M.E.M.P., Unsteady Measurements in a Separated and Reattaching Flow, *Journal of Fluid Mechanics*, Vol. 144, 1984, pp. 13-46.

[8] Tafti, D. K. and Vanka, S. P., A Three-Dimensional Numerical Study of Flow Separation and Reattachment on a Blunt Plate, *Physics of Fluids*, Vol. 3, No. 12, 1991, pp. 2887-2909.

[9] Hillier, R., Cherry, N. J., Pressure Fluctuations under a Turbulent Shear Layer. *Proceedings of the third Turbulent Shear Flow Symposium*, Davis, California, 1981, pp. 23–29.

[10] Abdalla, I. E. and Yang, Z., Numerical Study of a Separated-Reattached Flow on a Blunt Plate, AIAA JOURNAL, Vol. 43, No. 12, 2005, pp. 2465–2474.

[11] Lee, I., and Sung, H. J., Characteristics of wall pressure fluctuations in separated and reattaching flow over a backward-facing step, *Exp. Fluid*, Vol. 30, 2001, pp. 262-272.

[12] Castro, I. P., Haque, A., The Structure of a Turbulent Shear Layer Bounding a Separation Region, *Journal of Fluid Mechanics*, Vol. 179, 1987, pp. 439-468.

[13] Hudy, L. M., Naguib, A. M., Humphreys, W. M., Wall-pressure-array measurements beneath a separating/reattaching flow region, *Phys. Fluid*, Vol. 15, 2003, pp. 706-717.

[14] Ruderich, R. and Fernholz, H. H., An experimental investigation of a turbulent shear flow with separation, reverse flow and reattachment, *Journal of Fluid Mechanics*, Vol. 163, 1986, pp. 283–322.

[15] Yang, Z., and Voke, P. R., Large-Eddy Simulation of Boundary Layer Separation and Transition at a Change of Surface Curvature, *Journal of Fluid Mechanics*, Vol. 439, 2001, pp. 305-333.

[16] Ducoin, A., Loiseau, J., and Robinet, J., Numerical Investigation of the Interaction between Laminar to Turbulent Transition and the Wake of an Airfoil, *European Journal of Mechanics B/Fluids*, Vol. 57, 2016, pp. 231-248.

[17] Cantwell B. J., Organised Motion in Turbulent Flow. *Ann. Rev. Fluid Mech.*, Vol. 13, 1981, pp. 457-515.

[18] Hussain, A. K. M. F., Coherent Structures and Turbulence, *Journal of Fluid Mechanics*, Vol. 173, 1986, pp. 303-356.

[19] Robinson, S. K., *The Kinematics of Turbulent Boundary Layer Structure*, NASA Technical Memorandum TM 103859, 1991.

[20] Hussain, F. and Melander M. V., Understanding Turbulence via Vortex Dynamics, *Studies in Turbulence*, 1992, pp. 157-178.

[21] Yang, Z., Numerical Study of Instabilities in Separated-Reattached Flows, *Int. Journal of Comp. Meth. and Exp. Meas.*, Vol. 1, No. 2, 2013, pp. 116-131.

[22] McMullan, W. A. and Garrett, S. J., Initial Condition Effects on Large Scale Structure in Numerical Simulations of Plane Mixing Layers, *Phys. Fluids*, Vol. 28, 2016, p. 015111.

[23] Comte, P., Silvestrini, J. H., and Begou, P., Streamwise Vortices in Large-Eddy Simulation of Mixing Layers, *Eur. J. Mech. B/Fluids*, Vol. 17, No. 4, 1998, pp. 615-637.

[24] Browand F. K. and Trout, T. R., The Turbulent Mixing Layer: Geometry of Large Vortices, *Journal of Fluid Mechanics*, Vol. 158, 1985, pp. 489-509.

[25] Brown, G. L. and Roshko, A., On Density Effects and Large Structure in Turbulent Mixing Layers, *Journal of Fluid Mechanics*, Vol. 64, 1974, pp. 775-816.

[26] Perry, A. E. and Chong, M. S., On the Mechanism of Wall Turbulence, *Journal of Fluid* Mechanics, Vol. 119, 1982, pp. 173-217.

[27] Chernyshenko, S. I. and Baig, M. F., The Mechanism of Streak Formation in Near-Wall Turbulence, *J. Fluid Mech.*, Vol. 544, 2005, pp. 99-131.

[28] Schlatter, P., Brandt, L., de Lange, H. C., and Henningson, D. S., On Streak Breakdown in Bypass Transition, *Physics of Fluids*, Vol. 20, 2008, p. 101505.

[29] Watmuff, J. H., Pook, D. A., Sayadi, T., and Wu, X., Fundamental Physical Processes Associated with Bypass Transition, *Center for Turbulence Research, Proceedings of the Summer Program*, 2010, pp. 97-106.

[30] Deguchi, K. and Hall, P., Free-Stream Coherent Structures in Growing Boundary Layers: A Link to Near-Wall Streaks, *J. Fluid Mech.*, Vol. 778, 2015, pp. 451-484.

[31] Scarano, F., Benocci, C., and Riethmuller, M. L., Pattern Recognition Analysis of the Turbulent Flow Past a Backward Facing Step, *Phys. Fluids*, Vol. 11, No. 12, 1999, pp. 3808-3818.

[32] Giralt, F. and Ferre, J. A., Structure and flow pattern in turbulent wakes, *Phys. Fluids*, Vol. A5, No. 7, 1993, pp. 1783-1789.

[33] Hussain, A. K. M. F. and Hayakawa, M., Education of Large-Scale Organized Structures in a Turbulent Plane Wake, *Journal of Fluid Mechanics*, Vol. 180, 1987, pp. 193-229.

[34] Adrian, R. J. Meinhart, C. D., and Tomkins, C. D., Vortex Organization in the Outer Region of the Turbulent Boundary Layer, *J. Fluid Mech.*, Vol. 422, 2000, pp. 1-54.

[35] Wei, S. and Ning, T., Bursting Frequency in Turbulent Boundary Layers, *ACTA MECHANICA SINICA*, Vol. 4, No. 4, 1988, pp. 291-296.

[36] Gordeyev, S. V. and Thomas, F. O., Coherent Structure in the Turbulent Planar Jet. Part 2. Structural Topology via POD Eigenmode Projection, *J. Fluid Mech.*, Vol. 460, 2002, pp. 349-380.

[37] Hellstrom, L. O., Ganapathisubramani, B., and Smits, A. J., The Evolution of Large-Scale Motions in Turbulent Pipe Flow, *J. Fluid Mech.*, Vol. 779, 2015, pp. 701-715.

[38] Karaca, S. and Gungor, A. G., DNS of Unsteady Effects on the Control of Laminar Separated Boundary Layers, *European Journal of Mechanics B/Fluids*, Vol. 56, 2016, pp. 71-81.

[39] Gungor, A. G. and Simens, M. P., Transition to Turbulence in a Separated Boundary Layer with Spanwise Perturbations, *Procedia IUTAM*, Vol. 14, 2015, pp. 69-77.

[40] Abdalla, I. E. and Yang, Z., Numerical Study of the Instability Mechanism in Transitional Separating-Reattaching Flow, *International Journal of Heat and Fluid Flow*, Vol. 25, No. 4, 2004, pp. 593-605.

[41] Abdalla I. E., Yang, Z., and Cook, M., Computational Analysis and Flow Structure of a Transitional Separated-Reattached Flow over a Surface Mounted Obstacle and a Forward-Facing Step, *International Journal of Computational Fluid Dynamics*, Vol. 23, No. 1, 2009, pp. 25–57.

[42] Yang, Z., Large-eddy Simulation: Past, Present and the Future, *Chinese Journal of Aeronautics*, Vol. 28, No. 1, 2015, pp. 11-24.

[43] Piomelli, U., Large-Eddy Simulation: Achievements and Challenges, *Progress in Aerospace Sciences*, Vol. 35, 1999, pp. 335-362.

[44] Germano, P., Piomelli, U., Moin, P., and Cabot, W. H., A Dynamic Subgrid-Scale Eddy Viscosity Model, *Journal of Physics of Fluids*, Vol. A3, No. 7, 1991, pp. 1760-1765.

[45] Lilly, D. K., A Proposed Modification of the Germano-Subgrid-Scale Closure Method, *Physics of Fluids a-Fluid Dynamics*, Vol. 4, No. 3, 1992, pp. 633-635.

[46] Issa, R. I., Solution of the Implicitly Discretized Fluid Flow Equations by Operator-Splitting, *Journal of Comput. Phys*, Vol. 62, 1986., pp. 40–65.

[47] Castro, L P. and Epik, E., Boundary Layer Development after a Separated Region, *Journal of Fluid Mechanics*, Vol. 374, 1998, pp. 91-116.
[48] Yang, Z. and Abdalla, I. E., Effects of Free-Stream Turbulence on a Transitional Separated-Reattached Flow over a Flat Plate with a Sharp Leading Edge, *International Journal of Heat and Fluid Flow*, Vol. 30, No. 5, 2009, pp. 1026–1035.
[49] Le, H., Moin, P., and Kim, J., Direct Numerical Simulation of Turbulent Flow over a Backward-Facing Step, *Journal of Fluid Mechanics*, Vol. 330, 1997, pp. 349-374.
[50] Mabey, D. G., Analysis and Correlation of Data on Pressure Fluctuations in Separated Flow, *Journal of Aircraft*, Vol. 9, No. 9, 1972, pp. 642–645.
[51] Driver, D. M., Seegmiller, H. L., and Marvin, J. G., Time-Dependent Behaviour of Reattaching Shear Layer, *AIAA Journal*, Vol. 25, No. 7, 1987, pp. 914–919.
[52] Spazzini, P. G., Iuso, G., Onorato, M., Zurlo, N., and Di Cicca, G. M., Unsteady Behaviour of Back-Facing Step Flow, *Experiments in Fluids*, Vol. 30, 2001, pp. 551-561.
[53] Heenan, A. F., and Morrison, J. F., Passive Control of Pressure Fluctuations Generated by Separated Flow, *AIAA Journal*, Vol. 36, No. 6, 1998, pp. 1014–1022.
[54] Hunt, J. C. R., Wary, A. A. and Moin, P., Eddies, Stream, and Convergence Zones in Turbulent Flows, *Report in Center for Turbulence Research, Proceeding of Summer Program*, 1988, pp. 193-208.